Semi-Packed Micro Gas Chromatography Columns

Syed Aftab Ali

Thesis Submitted to the faculty of the
Virginia Polytechnic Institute and State University
in partial fulfillment of the requirements for the degree of

Master of Science
in
Electrical Engineering

Masoud Agah, Chairman
Robert W. Hendricks
Mehdi Ashraf-Khorassani

September 12, 2008
Blacksburg, VA

Keywords: Gas chromatography, MEMS, MicroGC, Separation Columns, Micro Analytical Systems.

Semi-Packed Micro Gas Chromatography Columns

Syed Aftab Ali

ABSTRACT

Separation of complex gaseous mixtures using gas chromatography (GC) is an important step in analytical systems for environmental monitoring, medical diagnosis, and forensic science. Due to its high resolving power, analysis speed, and small sample size, GC, has become the premier technique for separation and analysis of volatile and semi-volatile organic compounds. Miniaturization of analytical systems has become a major trend which is mainly driven by advancements in microfabrication techniques and a need for portable lab-on-a-chip systems for onsite monitoring. Microfabricated columns have been explored for applications in analytical processes like GC in several research studies. These microGC columns typically have open rectangular or open circular cross sections which is a result of the etching process utilized in the fabrication. This work reports the fabrication and performance of a new generation of silicon-on-glass micro-electro-mechanical systems (MEMS) based GC columns with microposts namely "semi-packed." These columns can be fabricated on a 2 cm^2-die for a 1 m-long channel or a 1 cm^2-die for a 25 cm-long channel. The semi-packed columns have a higher sample capacity as the overall surface area is larger than that of open rectangular columns of the same dimensions. The separation efficiency of these columns is also superior to that of open columns due to the presence of the microposts. As compared to conventional packed columns, the semi-packed columns show lower pressure drops and a more uniform flow profile, both of which contribute to, performance in terms of separation efficiency.

Acknowledgements

My deepest gratitude goes to my parents who made it possible for me to come to Virginia Tech to pursue my Bachelor's degree and their continued support through my graduate studies.

I would like to thank my advisor Dr. Masoud Agah for giving me an opportunity to work in this field and for his support and guidance throughout the course of this project. Thank you for your time and patience and for the motivation without which this would not have been possible.

I would also like to thank the members of my committee Dr. Robert Hendricks and Dr. Mehdi Ashraf-Khorassani and also Dr. Larry Taylor for his insightful comments.

I owe a special thanks to the VTMEMS group especially Bassam Al-feeli, Amin Zareian and Daniel Cho for their help in my experimental work.

My appreciation also goes to the members and users of MicrON Semiconductor Fabrication Laboratory, Donald Leber, for his support and patience during the launch of the facilities while I was learning to use them, also to Kevin Gantz, Mehdi Nikkhah and Krishna Vummidi for help with the equipment and processes.

Last but not the least I would like to thank my friend Josiah Ulfers who was always available with perceptive advice during our several conversations dealing with my writing and research.

Table of Contents

ABSTRACT ii
Acknowledgements iii
Table of Contents iv
List of Figures vi
List of Tables viii
CHAPTER 1: Introduction 1
1.1 : Gas Chromatography 1
1.2 : The GC Column 3
1.3 : Micro Gas Chromatography (μGC) 4
CHAPTER 2: Theory and Discussion 8
2.1 : Basic Definitions 8
2.2 : Theoretical Plate 9
2.3 : Rate Theory 11
2.3.1 : The A-Term: Eddy Diffusion 11
2.3.2 : The B-Term: Gas Diffusion 12
2.3.3 : The C-Term: Resistance to Mass Transfer 13
2.3.4 : The D-Term: Extra Column Effects 14
2.3.5 : Rectangular Columns 15
2.4 : Other terms Defining Separation Quality 16
CHAPTER 3: Design and Fabrication 18
3.1 : Semi-Packed μGC Column Design 18
3.1.1 : First Generation Design 19
3.1.2 : Second Generation Design 21
3.1.3 : Third Generation Design 22
3.2 : Fabrication 24
3.2.1 : Photolithography 24
3.2.2 : Deep Reactive Ion Etching 25
3.2.3 : Anodic Bonding 30
3.2.4 : Packaging 31
3.3 : Coating Procedure 32
3.3.1 : Deactivation 32
3.3.2 : Coating 33
CHAPTER 4: Results and Discussion 35
4.1 : Experimental Setup 35
4.2 : Separations 36
4.3 : HETP Measurement 39
4.3.1 : First Generation Columns 40
4.3.2 : Second Generation Columns 42
4.3.3 : Third Generation Design 43
4.4 : Sample Capacity 45
CHAPTER 5: Conclusion 46

5.1 : Future Work.....47
References..... 49

List of Figures

Figure 1.1: Schematic diagram and photograph of a GC system showing major components (Photo taken by Syed Ali) 2
Figure 1.2: Gas chromatogram of a mixture of pesticides 2
Figure 1.3: Schematic cross-section of a packed and an OT column 4
Figure 1.4: Components of a μGC system [1] 5
Figure 2.1: Typical chromatogram showing retention times 9
Figure 2.2: Schematic diagram demonstrating the concept of theoretical plates 10
Figure 2.3: Demonstration of eddy diffusion effect in packed columns 12
Figure 2.4: Longitudinal diffusion effect in a GC column 12
Figure 2.5: Parabolic velocity profile of the carrier gas velocity in an OT column 13
Figure 2.6: Effect of different band broadening terms as a function of average linear carrier gas velocity 15
Figure 3.1: SEM images showing the double-spiral square layout of an open rectangular column 19
Figure 3.2: Layout of the microposts in the first generation semi-packed channels 20
Figure 3.3: 3-D sections of a silicon-glass open rectangular MEMS channel (left) and a smi-packed channel 20
Figure 3.4: Velocity profiles of the open and semi-packed channels (a) under same pressure (b) with same maximum linear velocity 21
Figure 3.5: Velocity contour and profile for the square, diamond and long post (left to right) channels 22
Figure 3.6: Layout of the section of the third generation semi-packed design 23
Figure 3.7: Process flow for the fabrication of the GC columns; (a) Photolithography, (b) DRIE, and (c) Anodic bonding 24
Figure 3.8: Schematic of an RIE System 26
Figure 3.9: Etching and passivation steps in the Bosch process 27
Figure 3.10: SEM image of a post in a semi-packed channel demonstrating the scalloping effect of the Bosch process 27
Figure 3.11: SEM images of recipes during the optimization process with the final result at bottom-right 28
Figure 3.12: SEM images of sections of 1st generation (top-left), 2nd generation (top-right), and 3rd generation (bottom) etched semi-packed columns 29
Figure 3.13: Anodic bonding setup 30
Figure 3.14: SEM images of the silicon glass interface demonstrating the integrity of the seal 30

Figure 3.15: 1st generation semi-packed column after dicing and 3rd generation semi-packed column after being attached to the tubing 31
Figure 3.16: (a) Surface of the fused silica, (b) D4 in its cyclic form, and (c) after breakdown at 400 ˚C 33
Figure 3.17: Cross-linking of PDMS with the ATB free radical 34
Figure 3.18: SEM images of coating. Clockwise from top-left: middle of the column wall, closer to a corner, bottom of a post, and corner of silicon-glass interface. 34
Figure 4.1: Chromatogram showing the separation of the eight component mixture obtained by a 1st generation semi-packed column 37
Figure 4.2: Separation of alkanes at two temperatrure ramps with 2nd generation square 38
Figure 4.3: Backside of a column with the Pt/Ti heaters and temperature sensor 38
Figure 4.4: Separation of alkanes with 2nd generation open and semi-packed designs 39
Figure 4.5: Chromatogram used to plot the HETP points for efficiency calculation 40
Figure 4.6: HETP plotted for the 1st generation open and semi-packed columns 41
Figure 4.7: Velocity profile for the 1st generation channels simulated at their optimum velocities 42
Figure 4.8: HEPT for 2nd generation open and square semi-packed channels with optimal velocity profiles 43
Figure 4.9: Velocity profiles of 3rd generation channels at optimal conditions 44

List of Tables

Table 1.1: Types of columns employed in gas chromatography 3
Table 2.1: Comparisons of parameters among different theories 16
Table 3.1: Summary of third generation designs 23
Table 3.2: Parameters used in the final etching recipe 28
Table 4.1: Components in the standard mixture with their boiling points and purpose 37
Table 4.2: Summary of results in the 3rd generation columns 44
Table 4.3: Effects of increasing analyte amounts on the efficiency of the column 45

CHAPTER 1: Introduction

There is a strong trend towards the miniaturization of analytical systems. This trend has been aided by the advances in microfabrication technology. This has made possible the integration of mechanical and electrical systems on the micro-scale using silicon, aiding the development of these miniaturized systems. The pioneering work in the field of microelectromechanical systems (MEMS) based microfluidic devices was reported by Manz *et al.* [2] that established the field of micro total analytical systems (μTAS). There are several advantages of applying this technology to gas chromatography (GC) systems; the main one is the portability of μTAS making them suitable for field use. With fieldable analytical systems, the instrument can be taken to the sample as opposed to bringing the sample to the instrument. Due to the small nature of the device, μTAS would also have much lower power consumption as compared to conventional analytical systems. Lastly, μTAS can achieve faster analysis times as the entire system can be integrated as a lab-on-a-chip device [1, 3-5].

This chapter introduces the basic operation of a GC system followed by a discussion of conventional GC columns. Finally, μGC is introduced with a summary of research conducted by various groups in this field.

1.1: Gas Chromatography

Chromatographic separations were first achieved in the early 1900s on mixtures of gases and vapors using adsorbents like charcoal [6] and separations of plant pigments by liquid chromatography [7, 8]. Chromatography is based on a system of two phases, mobile and stationary, in which the components of a mixture are separated due to the relative distribution between the two phases [9]. GC is the form of chromatography that employs a gas as the mobile phase known as the carrier gas. The first work in GC was reported by James and Martin in 1952 [10] based on earlier work published by Martin and Synge in 1941 [11]. Figure 1.1 shows the setup of a conventional GC system comprising of a carrier gas tank, a wall-coated open tubular column which is enclosed in an oven, and a detector at the column outlet which is connected to a

data analysis system. Also shown in the figure is a photograph of a Hewlett Packard 5890 GC system with an HP 7673B autosampler injection system.

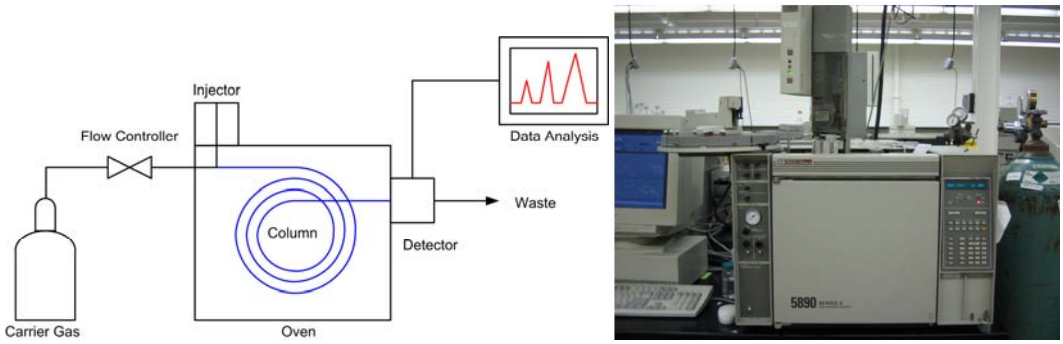

Figure 1.1: Schematic diagram and photograph of a GC system showing major components (Photo taken by Syed Ali)

When a sample is injected, it is first vaporized at the injector and then carried by the gas through the column. The components of the mixture are separated based on the principle of mass transfer between the stationary phase (the coating on the walls of the GC column) and the mobile phase (the carrier gas). The relative amount of time spent in the stationary phase with respect to that spent in the mobile phase is different for each component. Therefore, the compounds are separated as they travel through the column. The detector then generates an electronic signal consisting of peaks that identify the elution time and concentration of each component as it exits the column. Figure 1.2 shows the separation of a mixture of pesticides using a conventional column demonstrating the high resolving power of a GC system.

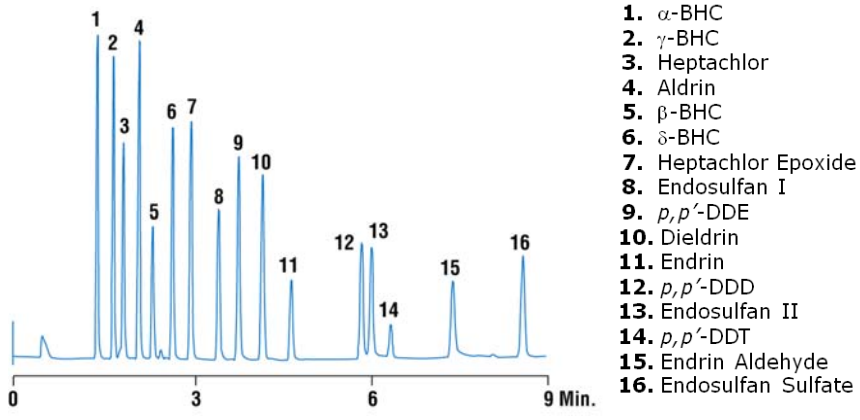

Figure 1.2: Gas chromatogram of a mixture of pesticides

1.2: The GC Column

The separation column is the central component of a GC system. The first columns employed in GC were made of metal and were packed with adsorbing materials that supported the stationary phase. These columns were found to be inefficient and the packing process was very time consuming. Glass columns solved some of the inertness problems associated with metal columns but had other issues like fragility. The invention of the capillary or open tubular (OT) column can be attributed to the work of Marcel J. E. Golay who demonstrated the theory and the high resolving power of these columns in 1958. The OT columns also went through a long evolutionary period until the invention of the fused silica capillary tubing in 1979 which is used universally at present in gas chromatography. The major attributes that make fused silica column superior to previous columns is their inertness and flexibility that metal and glass columns lack [12]. The evolution of these columns continues to take place to date. Table 1.1 lists the types of columns employed in GC and a brief description of each type of column.

Table 1.1: Types of columns employed in gas chromatography

Packed	Gas Solid Chromatography (GSC)	Solid stationary phase
	Gas Liquid Chromatography (GLC)	Liquid stationary phase (Gel)
Open Tubular (OT)	Wall Coated Open Tubular (WCOT)	Stationary phase supoorted by inner wall
	Support Coated Open Tubular (SCOT)	Stationary phase supported by a layer of adsorbent material on inner wall
	Porous Layer Open Tubular (PLOT)	Contains layer of porous solid adsorbent in inner wall

In spite of the popularity of WCOT fused silica columns, packed columns are still used in certain applications of GC that do not require high resolution. Packed columns offer a higher sample capacity, that is, they are able to process larger amounts of the analyte without loss of efficiency as compared to OT columns. This is because the packing material offers greater surface area which is able to support more of the stationary phase. Furthermore, methods that were previously validated on packed columns continue to use the same as it may not be economically feasible to validate a new method for capillary columns [13]. Figure 1.3 shows the cross sections of the WCOT and a packed column along with the stationary phase.

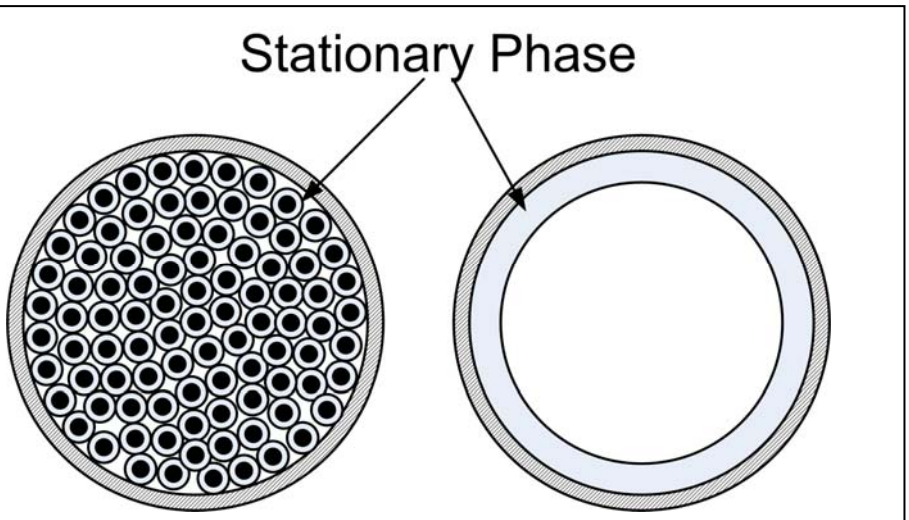

Figure 1.3: Schematic cross-section of a packed and an OT column

1.3: Micro Gas Chromatography (μGC)

As seen in Figure 1.1 gas chromatography systems are very bulky due to the oven and carrier gas tank. The temperature cycling of these large ovens makes these systems very power hungry when higher temperatures are required. Additionally, fast temperature cycling cannot be achieved for these systems making it difficult to achieve fast separation times. Though μGC columns cannot provide the high resolution that has been achieved by conventional columns (see Figure 1.1), they have the advantage of μTAS in being fast, portable and less power consuming. Figure 1.4 shows the typical components of a μGC system comprising of a preconcentrator, a microcolumn, and a detector along with other peripherals. The preconcentration stage is necessary because the samples available in the environment may be present in low concentrations. This is not the case for traditional GC where the samples are prepared to obtain the required concentration.

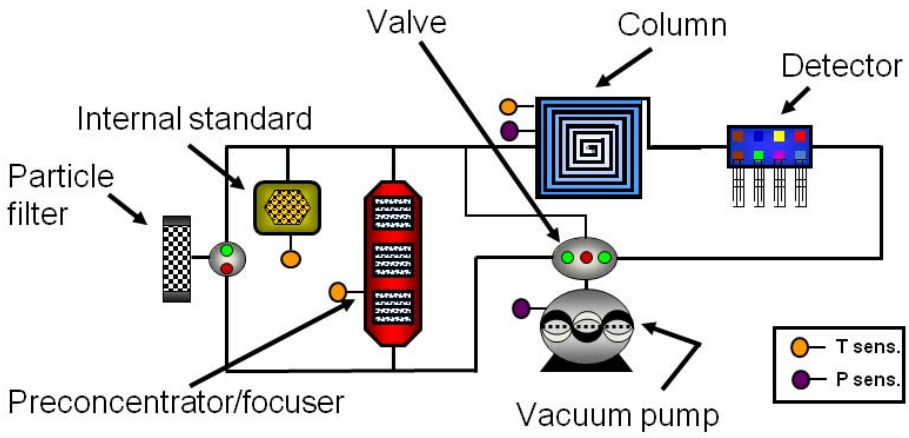

Figure 1.4: Components of a µGC system [1]

The use of MEMS technology to develop miniaturized GC columns has been in progress in several laboratories. Early work on µGC was performed at Stanford University and reported in 1979 [14]. These columns (1.25 m-long, 200 µm-wide and 30-µm deep) were roughly rectangular, laid out in a spiral format, and sealed with an anodically bonded Pyrex wafer. A mixture of hydrofluoric acid (HF) and nitric acid (HNO_3) was used for the wet etching. These polydimethylsiloxane (PDMS) coated columns successfully separated a mixture of nitrogen, pentane and hexane in under five seconds and yielded efficiencies of ~300 to 1500 plates/m. A more complex mixture comprising of eight components which included both straight chain and chlorinated hydrocarbons was also separated in ten seconds.

Reston and Kolesar reported a silicon-based microfabricated GC column in 1994 [15-17]. These 0.9 m-long (300 µm-wide and 10-µm deep) columns were fabricated in a similar manner to that mentioned previously but employed a novel way of coating the column which used copper phthalocyanine (CuPc) as the stationary phase. These columns accomplished a separation of ammonia (NH_3) and nitrogen dioxide (NO_2) which are common pollutants in 30 minutes at 80˚C.

Researchers at Sandia National Laboratories fabricated silicon-glass microcolumns of varying dimensions using both wet and plasma etching techniques in 1998 [18]. The plasma can etch silicon anisotropically resulting in highly vertical sidewalls. These columns were coated with polydimethylsiloxane (PDMS) as the stationary phase. Separations of dimethyl methyl phosphate (DMMP, a nerve agent stimulant), Toluene and Xylene (typical interferents) were demonstrated in under 30 seconds.

Wiranto *et al.* fabricated 1.25 m long silicon-glass columns (100 μm-wide and 20 μm-deep) using wet etching techniques (HNO_3 and HF) with PDMS as the stationary phase [19]. Separations of hydrocarbon mixtures (C_{11} to C_{16}) were accomplished in under 1.25 min at an isothermal temperature of 150˚C. The efficiency of these columns ranged from 850 to 1754 plates/m.

The thermal cycling capabilities of microcolumns were studied on parylene based columns by Noh *et al.* to achieve rapid temperature ramps [20]. The fabrication process involved coating the etched silicon microchannels and Pyrex wafers with parylene. Instead of anodic bonding, parylene/parylene thermal bonding was used to seal the channels. The bulk silicon and pyrex material was etched away with potassium hydroxide (KOH) which resulted in freestanding parylene columns. This reduces the thermal mass of the channels for faster thermal cycling which is also helped by the low heat capacity of parylene. A deposited gold film was used as the heating element and the column was heated up to 100˚C in 40 seconds while consuming only 50 mW of power.

Lambertus *et al.* conducted a detailed investigation to plot the efficiency of silicon-glass columns at the University of Michigan [21]. These columns were 3 m-long, 150 μm-wide and 240 μm-deep with rectangular cross sections. The efficiency was calculated to study the effects of oxide on the coating, polar or non-polar stationary phases, and the carrier gas used (air and hydrogen). The best results were obtained with non-oxide columns coated with a non-polar stationary phase (PDMS) using air as the carrier gas. These columns were able to generate more than 2700 plates/m. Separations of complex 20 component mixtures were obtained using temperature programming and also at isothermal temperatures. These columns were also integrated with microfabricated preconcentrators, sensor array detectors, on-chip heaters, pressure and temperature sensors to separate complex mixtures while using less power and achieving higher portability [22, 23]. After the development of new coating methods, the 3 m long columns were able to generate over 4000 plates/m [24] and separations of chemical warfare agent (CWA) simulants were achieved with 25 cm long columns in less than 10 seconds. These CWA simulants included cyclohexanone, DMMP, 2-nitrotoluene and methylsalicylate. These chemicals are stimulants for C-4, sarin nerve gas, TNT and mustard gas respectively [1]. Agah *et al.* also developed a new buried channel process to create ultra-low mass released structures for

microcolumns comprising of stress-free PECVD oxynitride films [25]. These columns were able to separate multi-component mixtures utilizing only 10 mW to operate at 150˚C in vacuum.

Bhushan *et al.* fabricated nickel μGC columns using the LiGA technique in which a patterned layer of polymethylmetacrylate (PMMA) was used as a mold for electroplated Ni [26, 27]. The PMMA layer was later removed by heating, releasing the nickel columns to form the channels with high aspect ratios (50 μm-wide, 700-800 μm-deep). The high aspect ratio takes full advantage of rectangular channels in terms of efficiency, which is improved by the narrow width, without impeding flow rate or capacity due to the large depth.

Though microfabricated columns do not have the efficiency achieved by conventional columns, μGC has a promising future in a wide range of applications. For example, the detection of chemical and biological warfare agents would require a low cost, high performance miniature GC so that it can be operated in the field. Environmental monitoring is another major application for μGC as it is easier to collect and analyze the samples in the field as opposed to bringing them to the lab for analysis. Finally, μGC systems can also be developed for use in the field of medicine for breath analysis to detect bio-markers that indicate diseases. Currently, Sandia National Labs have developed a handheld system named MicroChemLab® that comprises of a preconcentrator, a separation column and a surface acoustic wave (SAW) sensor [28]. This product was mainly developed for environmental monitoring for defense purposes.

CHAPTER 2: Theory and Discussion

There are several dynamic processes occurring inside a column as the mixture travels through it which affect the performance of the column and the resulting chromatogram. The first attempts to explain these processes led to the plate theory which was based on an equilibrium model. This model, however, could not explain the non-equilibrium conditions in the column nor could it explain the factors that affecting the broadening of the chromatographic peaks commonly referred to as band broadening. Another model, known as the rate theory, was developed which explained the kinetic factors effecting band broadening in 1956 for packed columns [29]. This model was later modified to fit open tubular columns as well by Golay in 1958 and is still used to measure the performance of GC columns.

This chapter introduces the fundamental theories behind GC starting with some basic definitions. The concept of plates and the rate theory are also explained which determine the efficiency of the separation. Finally, some other terms that determine separation quality are described.

2.1: Basic Definitions

This section explains some of the common terms and definitions that are commonly used in GC. The first of these terms is the hold-up time (t_M), which is the time taken by an unretained component to travel the length of the column. Components like air and methane interact minimally with the stationary phase and hence are considered unretained. These unretained components can be used to measure the average linear carrier gas velocity in the column ($\bar{u}$) or as solvents for the gas mixture samples. Retention time (t_R), also known as the elution time, is the time it takes for retained components to exit the column. In many chromatographic calculations the adjusted retention time (t'_R) is taken into account which is obtained by subtracting the hold-up time from the retention time. These terms are explained graphically in Figure 2.1.

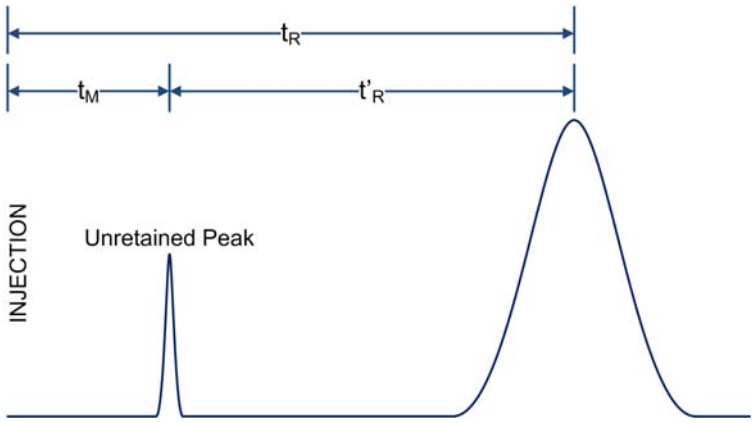

Figure 2.1: Typical chromatogram showing retention times

Another important term in GC is the retention factor (k), which is important in determining the efficiency of the separation. This term is calculated by dividing the adjusted retention time by the hold-up time (t'_R/t_M) and is independent of the carrier gas velocity. These terms will be used extensively in defining other complex relationships in GC systems.

2.2: Theoretical Plate

The GC column can be divided into a number of theoretical plates, where, a plate is the smallest section of the column where an analyte can achieve equilibrium between the two phases. The length of each plate is termed as height equivalent to a theoretical plate (HETP) [11]. The concept of a theoretical plate is explained schematically in Figure 2.2 which depicts a column with five theoretical plates. The mobile phase is represented by the white portion and the stationary phase by blue. The sample consists of two components, one of which is soluble in the stationary phase (black dots) and the other is insoluble (grey dots), and is unretained. During each step, the portion of the components in the mobile phase travels to the next plate and then equilibrium is achieved for each soluble component within a single plate. As a result of these travels and equilibrium steps, the components distribute themselves in a Gaussian profile along the column. It can be seen that in order to enhance the resolution of the two components more plates are required. This can be achieved either by using a longer column or one with a smaller plate height.

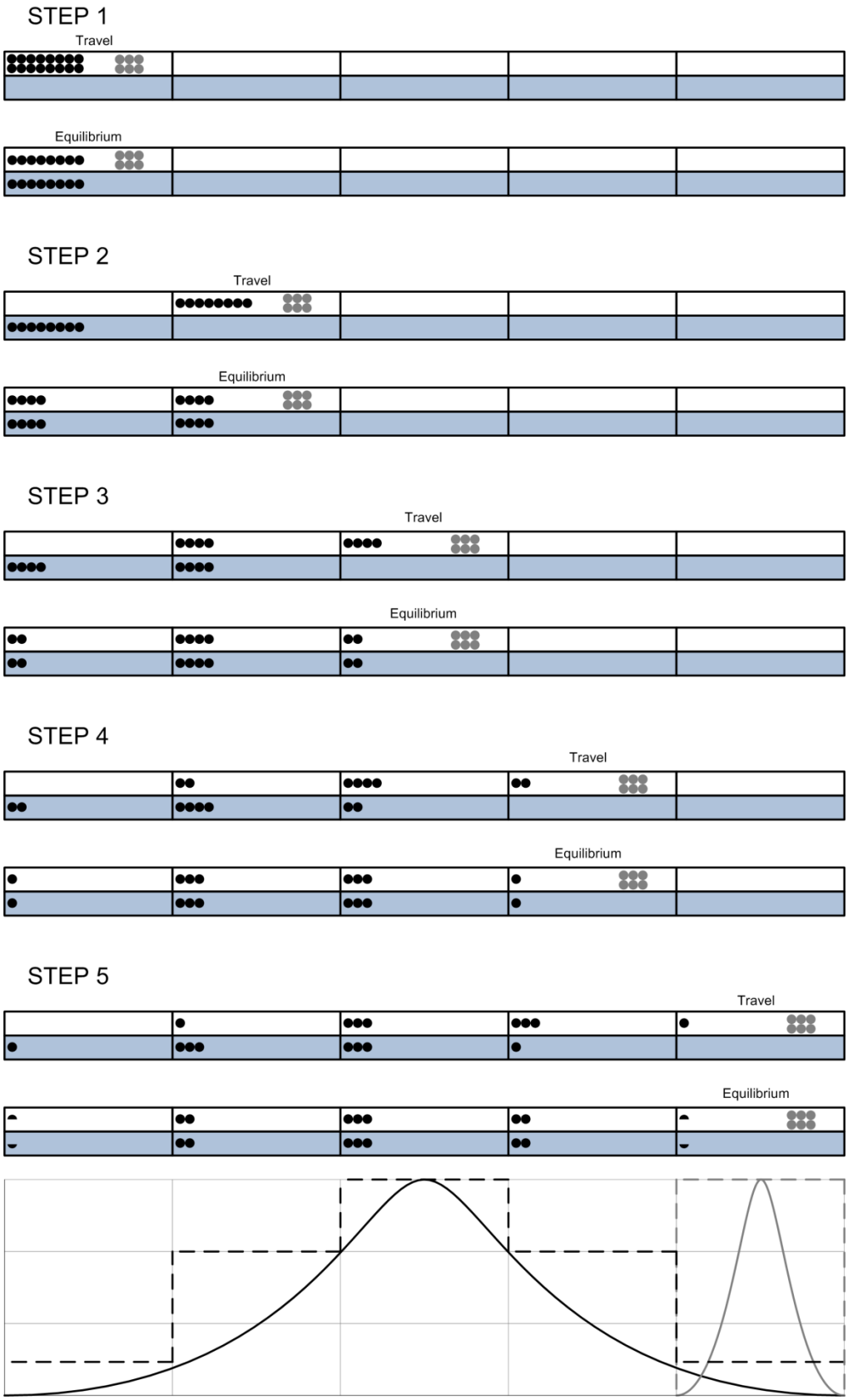

Figure 2.2: Schematic diagram demonstrating the concept of theoretical plates

Due to the Gaussian profile of the eluted peak, the total number of plates for the column can be calculated based on the standard deviation (σ) and mean or the elution time (t_R) of the peak [13]:

$$N = \left(\frac{t_R}{\sigma}\right)^2 = 16\left(\frac{t_R}{w_b}\right)^2 = 5.54\left(\frac{t_R}{w_h}\right)^2 \quad (2.1)$$

Here, w_b and w_h are the peak widths at the base and at half height respectively. The HETP can then be calculated using the length of the column:

$$HETP = \frac{L}{N} \quad (2.2)$$

The HETP is a better measure to compare efficiencies of different columns as it is independent of the length. It is desirable to achieve a large N or a small HETP for high resolution separations.

2.3: Rate Theory

The plate number or the height of the plate, though a good measure of efficiency, do not give a clear insight to the kinetics taking place inside the column that lead to band broadening. The original equation based on the rate theory is known as the van Deemter equation for packed columns which relates the HETP and the average linear carrier gas velocity ($\bar{u}$):

$$HETP = A + \frac{B}{\bar{u}} + C \cdot \bar{u} + D \cdot \bar{u}^2 \quad (2.3)$$

where *A*, *B*, *C* and *D* represent different phenomena that cause band broadening. The equation was later modified to the Golay equation for open tubular columns which excluded the A-term. The D-term was added later to consider the extra column effects which are prevalent in short columns with relatively high carrier gas velocities. These terms are explained in the following sections.

2.3.1: The A-Term: Eddy Diffusion

The *A*-term represents the eddy diffusion effect in packed columns. This occurs due to the non-uniform size and packing order of the columns that makes paths of different lengths along the column causing band broadening. This effect is demonstrated in Figure 2.3 where three molecules of the same component experience band broadening due to eddy diffusion [13]:

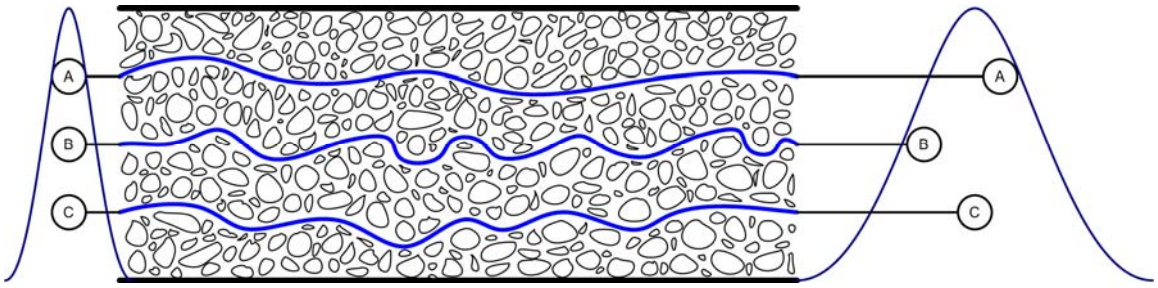

Figure 2.3: Demonstration of eddy diffusion effect in packed columns

This term depends on the size of the packing material (d_p) and the packing factor (λ) which in turn is primarily affected by the uniformity in size and packing [13]:

$$A = 2\lambda d_p \tag{2.4}$$

2.3.2: The B-Term: Gas Diffusion

The *B*-term represents the longitudinal diffusion. This is when the solute in the carrier gas diffuses from high concentration to low concentration as shown in Figure 2.4 where the peak broadens as the time increments from T1 to T3 assuming zero carrier gas velocity [13].

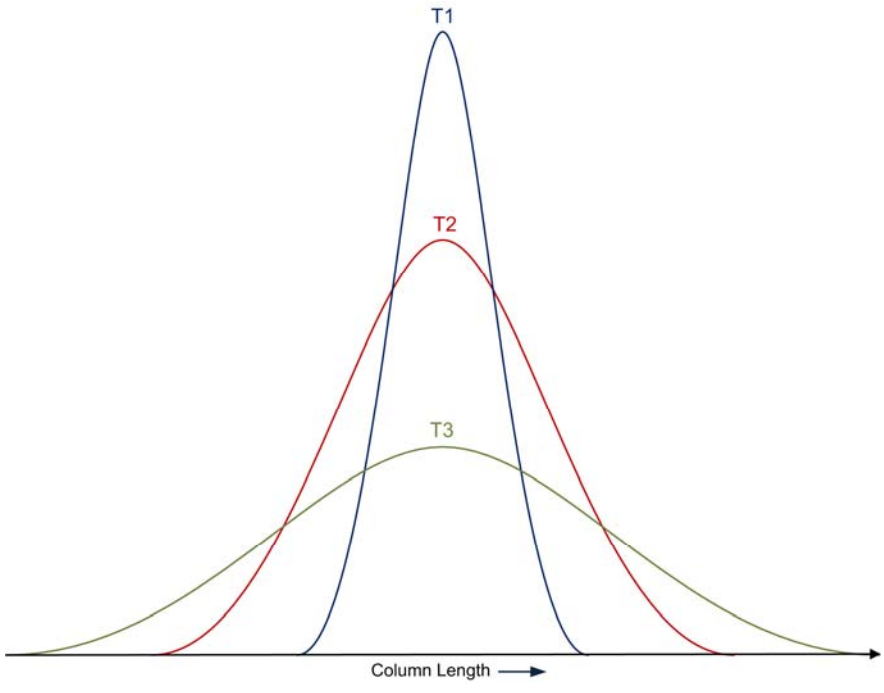

Figure 2.4: Longitudinal diffusion effect in a GC column

This term is defined separately for open tubular and packed columns due to the presence of a tortuosity factor (γ) in packed columns that again accounts for the nature of the packed bed. The

B-terms for open tubular and packed columns are given by equations (2.5) and (2.6) respectively [30].

$$B = 2D_G \tag{2.5}$$

$$B = 2\gamma D_G \tag{2.6}$$

D_G is the diffusion coefficient for the solute in the carrier gas. It depends on the type of carrier gas used and its effect reduces with the increase in carrier gas velocity.

2.3.3: The C-Term: Resistance to Mass Transfer

The *C*-term represents resistance to mass transfer and can be divided into two parts, C_M for mass transfer in the mobile phase and C_S for mass transfer in the stationary phase. Mass transfer in the stationary phase can be explained with reference to Figure 2.2, in which, during the travel step the molecules of the solute must distribute themselves to obtain equilibrium. The faster this transfer takes place the lower the C_S-term is thus causing lesser band broadening. Mass transfer in the mobile phase is due to different velocities of the carrier gas which is caused by the laminar flow resulting in a parabolic velocity profile across the width of the channel as shown in Figure 2.5 [13]:

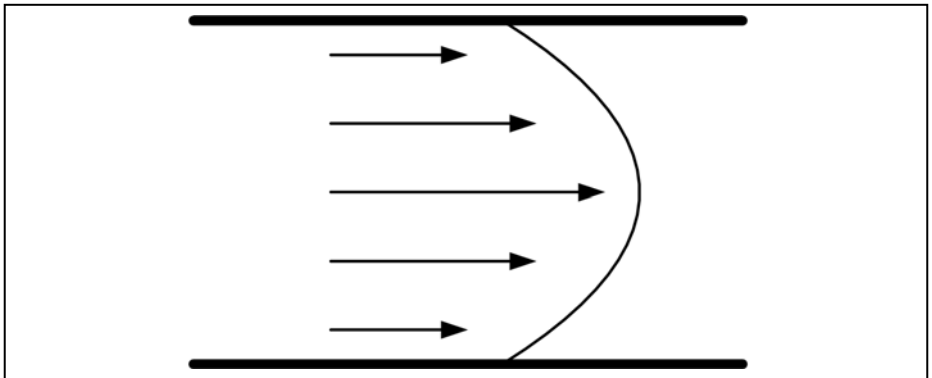

Figure 2.5: Parabolic velocity profile of the carrier gas velocity in an OT column

This effect is more prominent in open tubular columns as the mass transfer distances are larger but is also present in packed columns. The *C*-terms for both kinds of columns are given in the following equations [13, 31]:

$$OT\ C_S = \frac{2kd_f^2}{3(1+k)^2 D_S} \tag{2.7}$$

$$OT\ C_M = \frac{(1 + 6k + 11k^2)r_C^2}{24(1 + k)^2 D_G} \tag{2.8}$$

$$Packed\ C_S = \frac{8kd_f^2}{\pi^2(1 + k)^2 D_S} \tag{2.9}$$

$$Packed\ C_M = \frac{\omega d_p^2}{D_G} \tag{2.10}$$

D_S is the diffusion coefficient of the solute in the stationary phase. This term needs to be larger for faster mass transfer as explained earlier. ω is the obstruction factor which is a function of the packing and r_c is the radius of the capillary columns.

2.3.4: The D-Term: Extra Column Effects

In the case of short columns with relatively high average linear carrier gas velocities, another term responsible for band broadening appears which takes into account the extra column effects also known as instrumental contribution. This specially applies to MEMS-based columns that are in the order of a few meters in length. When the sample is injected, the width of the plug cannot be ignored in these cases as opposed to traditional columns that are usually very long. These effects are incorporated into the *D*-term which depends on the total instrumental dead time or the initial plug width (Δt) and the total length of the column (L) [24, 32]:

$$D = \frac{\Delta t^2}{L(k + 1)^2} \tag{2.11}$$

All these terms contribute to the broadening of the original sample plug injected as it travels through the column. As the contribution of each term depends on the average carrier gas velocity ($\bar{u}$), there is a unique value of $\bar{u}$ at which the HETP is found to be minimum known as the optimum carrier gas velocity ($\bar{u}_{opt}$) as illustrated in Figure 2.6.

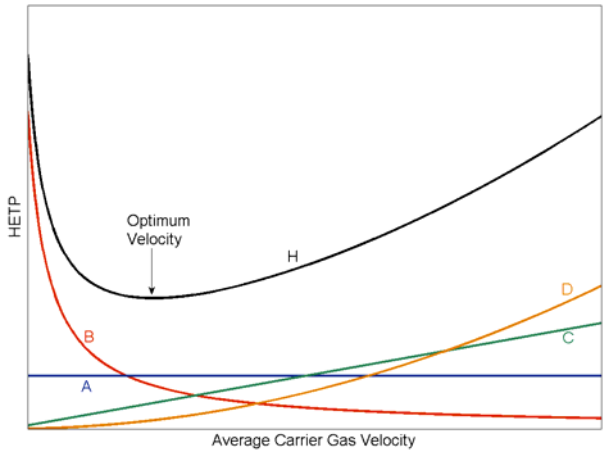

Figure 2.6: Effect of different band broadening terms as a function of average linear carrier gas velocity

2.3.5: Rectangular Columns

Rectangular columns were first investigated in [33-35] as they had the added advantage of providing two independent degrees of freedom with height and width. This allows the HETP to be adjusted without greatly affecting the carrier gas flow and the sample capacity. Rectangular µcolumns became popular after deep reactive ion etching (DRIE) and LiGA (lithography, electroplating and molding) techniques were developed to fabricate these channels. The HETP equation for open rectangular (OR) channel is similar to OT channels except for the C_M term which is significantly affected by the geometry of the column. This is due to the fact that the average linear velocity ($\bar{u}$) is derived separately for rectangular columns which affects coefficients to the retention factor in the equation [36]:

$$OR\ C_M = \frac{X + Yk + Zk^2}{96(1+k)^2} s^2 \qquad (2.12)$$

where s is the characteristic dimension of the column which can either be the width or the depth depending on the aspect ratio of the column. The coefficients X, Y and Z are influenced by the aspect ratio of the channel and the way $\bar{u}$ is defined. Early work on the definition of C_M assumed large aspect ratios and neglected the effects of the column sidewall [33, 37-41]. Spangler demonstrated the effects of the aspect ratio on the HETP but did not contain an explicit formula for the effects of the aspect ratio [42-44]. The effect of arbitrary aspect ratios on the HETP was reported by Ahn *et al.* and Liang *et al.* where numerical data from various aspect ratios was collected and regression analysis was performed to obtain a relationship [36, 45]. Each of these

works employed a slightly different method to model the flow in the column and hence obtained different results for the three coefficients as summarized in Table 2.1.

Table 2.1: Comparisons of parameters among different theories

	AR	X	Y	Z
Liang *et al.*	1	0.714	3.68	5.52
	∞	0.9143	8.229	23.31
Ahn *et al.*	1	1.608	9.22	15.61
	∞	7.269	41.11	65.84
Spangler	∞	0.9	2	35
Giddings *et al.*	∞	0.9	8.2	23
Golay	∞	0.9	8.2	23

2.4: Other terms Defining Separation Quality

Effective Plate Number: When determining the plate number for analytes with low retention factors, the hold-up time needs to be taken into account. Hence, the effective plate number is calculated using the adjusted retention time (t'_R) instead of the retention time (t_R). The plate number and the effective plate number converge as the retention factor increases.

Resolution: This term is used to express the degree of separation between two adjacent peaks and is defined by:

$$R_S = \frac{t_{R2} - t_{R1}}{\frac{w_{b1} - w_{b2}}{2}} \tag{2.13}$$

The subscripts 1 and 2 denote the first and second peak, respectively, and w_b is the width of the peak at the base. A resolution of 1.5 denotes the two components are separated almost completely with only 2% overlap [46].

Peak Number: This measures the total separating power of the column, that is, the number of peaks which the column has the capacity to resolve.

$$PN = \frac{R_s}{R_s^*} - 1 \tag{2.14}$$

where R_s is the resolution that separates two peaks and R_s^* is the desired resolution with which *PN* peaks will fit between the first two peaks.

Sample Capacity: This is the measure of the amount of analyte that can be injected into a column without overloading it, that is, saturating the stationary phase [47]. The overloading causes a decrease in the efficiency of the separation and hence care must be taken to avoid it. The sample capacity depends on the mass of the stationary phase which in turn is a product of the surface area of the column and the thickness of the stationary phase. Open tubular columns have very limited sample capacity as compared to packed columns due to their smaller surface area.

Peak Symmetry: Unsymmetrical peaks are an indication of problems within the column. For instance, tailing indicates an unstable stationary phase or active sites in the column and a leading peak is often an indication of overloading. A good quality column elutes highly symmetrical Gaussian peaks.

Analysis Time: This is the total time to separate a sample indicated by the elution of the last peak. The analysis time can be manipulated by either increasing the carrier gas velocity, or, by introducing temperature programming often at the cost of a decrease in resolution.

CHAPTER 3: Design and Fabrication

The main motivation behind the design was to take advantage of MEMS fabrication technologies and optimize the column configuration to improve the sample capacity and efficiency of the microcolumns and, at the same time, avoiding large pressure drops as experienced in conventionally packed columns. Muticapillary columns, which consist of several narrow capillary channels that run in parallel, are one way of achieving higher efficiencies without sacrificing sample capacity or pressure drop [48-50]. Semi-packed columns, however, provide a single volume for the gas to flow making it easier to coat them and also avoiding the drop in efficiency due to the differential flows among the capillaries that may exist in multicapillary columns. The introduction of the microposts in the channels attains columns that are hybrids between open (wide and narrow), packed, and multicapillary columns. As it is possible to control the size, shape, spacing, and number of the posts very precisely using microfabrication techniques, an ideal configuration for both sample capacity and efficiency can be achieved. This chapter discusses the initial design of the semi-packed column followed by the fabrication and coating methods used in the finished column.

3.1: Semi-Packed μGC Column Design

Closely packed collocated monolithic microstructures have been investigated for liquid chromatography (LC) and capillary electrophoresis (CE) that resemble the packed columns favored by these applications [51-57]. These microstructures are used to create very narrow channels that have dimensions in the order of a few microns and have unordered or staggered configuration that promotes inter-channel mixing beneficial to these applications. On the other hand, studies on MEMS GC columns have been mainly focused on open channels as they provide much better efficiency and lower pressure drops. Introducing such microposts that are larger and spaced further apart provides unique advantages to GC columns in terms of sample capacity and separation efficiency.

3.1.1: First Generation Design

The layout of the semi-packed columns was based on the double-spiral square layout reported for open columns as shown in the SEM images of Figure 3.1. Although several results have been reported for the effects of the column geometry on the band dispersion in case of electro kinetically driven CE systems [58-62] due to sidewall effects, studies show similar effects can also be applied to pressure driven systems as examined for LC systems [52, 57, 63]. One study reports the effects of the layout of the channel on the HETP of the column in μGC systems and shows a serpentine layout to have a higher efficiency than a spiral one [64]; however, an extensive study has not been made to investigate the issue. The double-spiral square was mainly chosen to compare the results to previously published μGC columns that used the same layout [65].

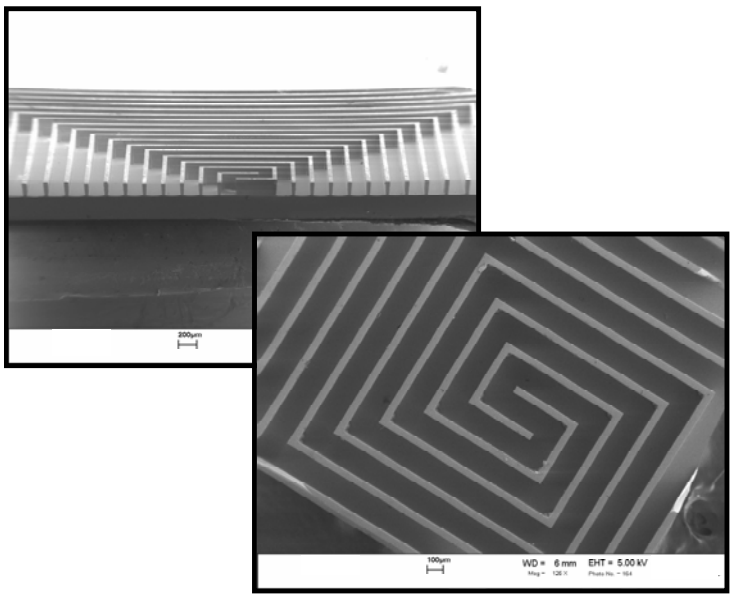

Figure 3.1: SEM images showing the double-spiral square layout of an open rectangular column

The semi-packed design comprised of square posts that are 20 μm on the side and were spaced 30 μm apart embedded in a channel 1 m-long, 150 μm-wide and 180 μm-deep. Figure 2.2 shows the dimensional details of the column layout.

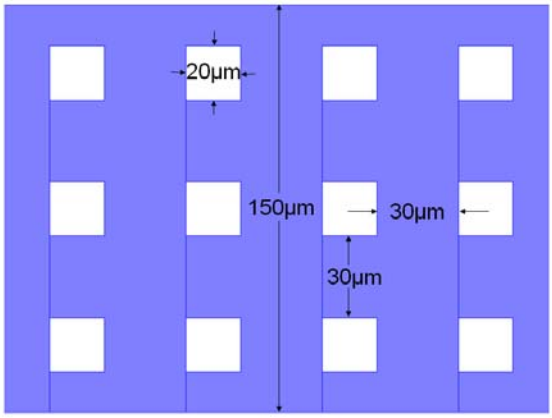

Figure 3.2: Layout of the microposts in the first generation semi-packed channels

This increased the overall surface area of the semi-packed chip to about 15 cm^2 which is twice that of an open rectangular column with the same dimensions. Furthermore, the effective radius of the channel decreased to 120 µm from 150 µm. This layout was drafted in CoventorWare which was then used to create a 3-D model of a section of the channels as shown in Figure 3.3.

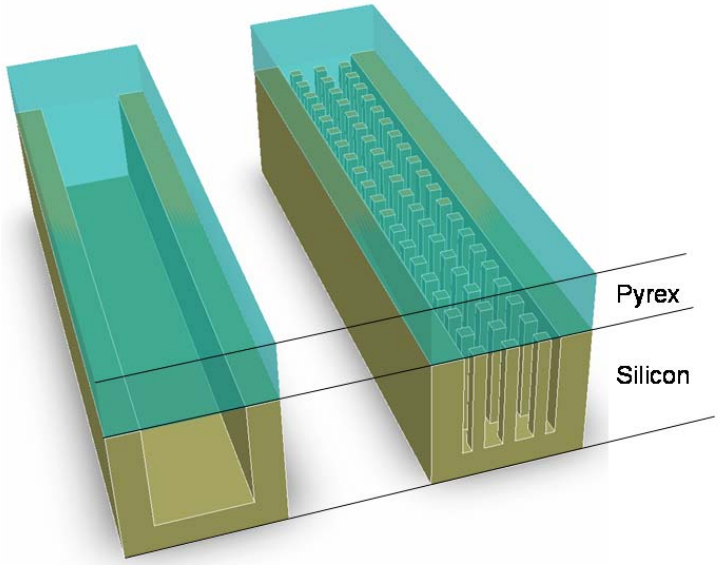

Figure 3.3: 3-D sections of a silicon-glass open rectangular MEMS channel (left) and a smi-packed channel

This model was used as a mold to create a mesh model of the space inside the channel to simulate the flow profiles of the carrier gas in the channels using finite element analysis. Figure 3.4(a) shows the velocity profiles generated by applying a pressure of 2 Pascal for a 1 mm long

channel and Figure 3.4(b) shows a simulation with the same maximum linear velocity. In the second case, the pressure drop was 0.1 psi/m in the open channel and 3 psi/m in the semi-packed channel. Decreasing the inlet pressure reduces the average linear carrier gas velocity and the variation in the velocity profile and hence the C_S-term. However, at lower velocities the effects of B-term greatly increase the HETP (see Figure 2.6). With the new semi-packed configuration, it is possible to achieve a lower minimum HETP as compared to open MEMS columns because of the new velocity profile characteristics. It should also be noted that this configuration of the square posts yields a flow profile that mimics a multicappilary columns as there is minimal flow between the posts along the length of the channel.

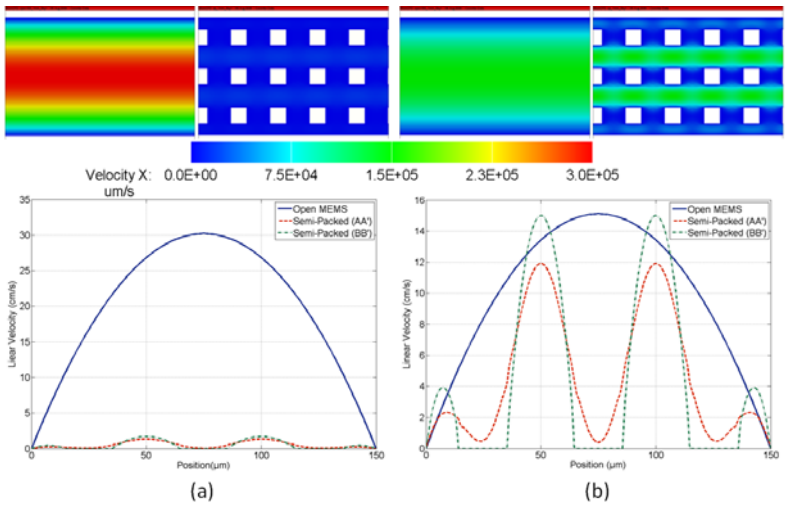

Figure 3.4: Velocity profiles of the open and semi-packed channels (a) under same pressure (b) with same maximum linear velocity

3.1.2: Second Generation Design

The second generation of semi-packed columns was designed to investigate how the post shape affects the flow of the carrier gas around it for optimum efficiency. Three designs were considered with square, diamond and long hexagonal posts. The three designs show different pressure drops and velocity variation. Another difference among the designs is the flow path of the molecules within the channel as seen in Figure 3.5 which shows the velocity contour and paths for the three designs.

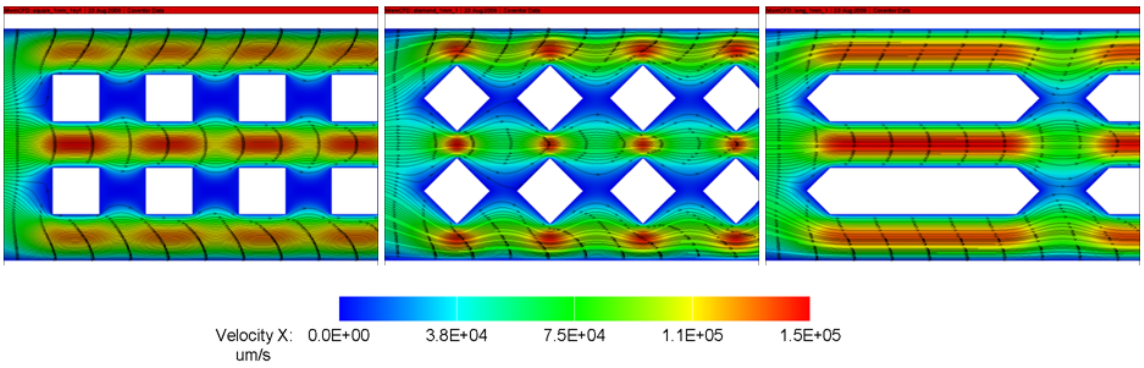

Figure 3.5: Velocity contour and profile for the square, diamond and long post (left to right) channels

The pressure drops in the channel were 2.81 psi/m, 3.07 psi/m, and 2.86 psi/m for the square, diamond, and long designs, respectively, for a maximum velocity of 15 cm/s. The diamond posts offer lesser zones with high velocity but have a higher pressure drop and the path of the molecules is more tortuous. The long posts offer the least total mass transfer distance and also a lower pressure drop compared to diamond posts. These columns were designed to give an idea about the effects of pressure drop, mass transfer distances and the path of the analyte on the performance of the channel. In order to maximize the amount of chip per wafer the length of the columns was decreased to 25 cm which made each chip area about 1 cm^2 with the double square spiral layout.

3.1.3: Third Generation Design

The third generation design investigates the effect of the post configuration on the efficiency of the column. A major change in this design was to use a serpentine layout instead of the double spiral layout. Early studies have shown the serpentine layout to have better efficiency [64] but the main reason behind this change was to make easy the process of drafting the layout. This layout made it possible to construct the column as a compilation of smaller sections which made the creation of the final output file for the mask faster. The second generation design took almost a day and a half to compile whereas the new layout took under a minute because it was quicker to compile the columns that were constructed with references of smaller sections. The length of the column was also changed back to one meter since the second generation design did not give a considerable difference in the performance. The columns were tested in a conventional GC oven which required connecting tubing around 35 cm in length. The 25 cm-long columns were too

short compared to the tubing for their effects to be dominant. The third major aspect of the design was the round posts as it was considered advantageous to eliminate any corners in the channel to achieve better coating performance.

Six designs were chosen to demonstrate the effects of post spacing, number of posts, and effective diameter. Two open rectangular designs were also incorporated to compare them to semi-packed channel. The design summary of the columns is given in Table 3.1.

Table 3.1: Summary of third generation designs

	Total Width	Min. Width	Effective Width	Post Spacing	Posts per Row
OR90	90	90	90	N/A	N/A
OR120	120	120	120	N/A	N/A
SP1	150	90	126	20	3
SP2	150	90	134	40	3
SP3	190	110	158	20	4
SP4	190	110	169	40	4

The total width of the channel is the outer width and the minimum width is the point at which the channel is narrowest between the posts. The effective width is calculated by averaging the width along the length of the channel giving the semi-packed channels a smaller effective width than their total width. In order to compare the semi-packed design to open rectangular channels, two open channels with the effective width and minimum width of the SP1 design, seen in Figure 3.6, have also been designed.

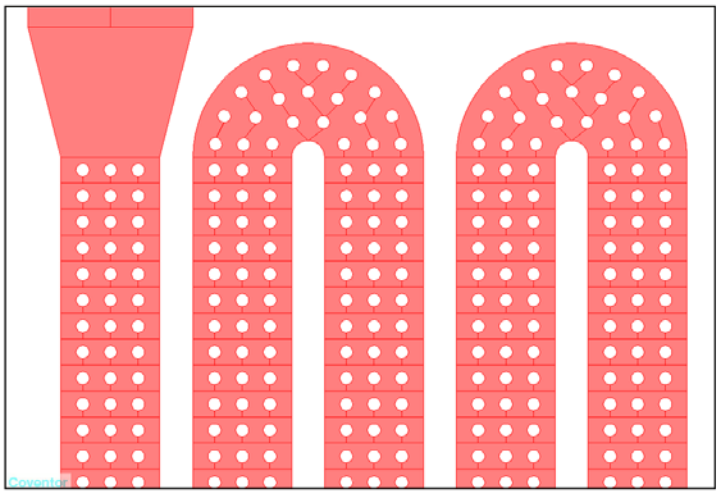

Figure 3.6: Layout of the section of the third generation semi-packed design

3.2: Fabrication

The fabrication of the devices involves semiconductor processing technology and utilizes silicon as a substrate for the channels and Pyrex to seal them. The three major steps of the process include photolithography, where the pattern is created on a photosensitive polymer called photoresist (PR); deep reactive ion etching (DRIE), a process by which the channels are anisotrpocially etched; and anodic bonding the Pyrex substrate to the silicon channels. These processes are summarized in Figure 3.7.

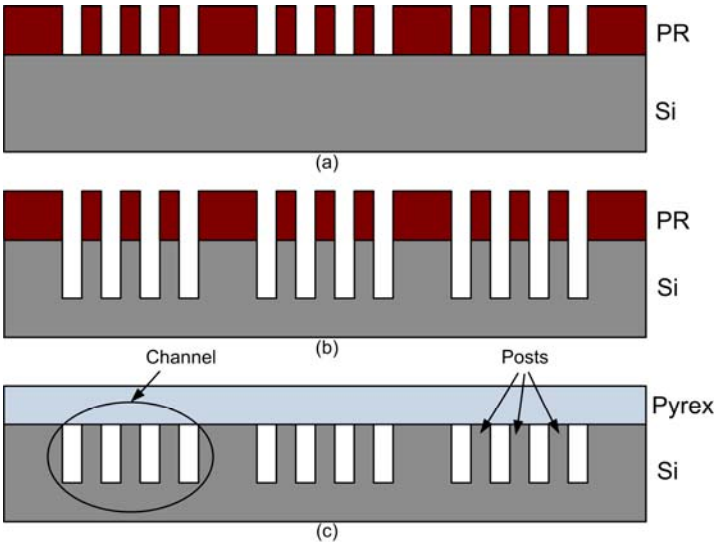

Figure 3.7: Process flow for the fabrication of the GC columns; (a) Photolithography, (b) DRIE, and (c) Anodic bonding

After fabrication, the channels were diced and attached to fused silica tubing to interface them with a conventional GC oven for testing. The following sections describe in detail each of the processes involved in the fabrication.

3.2.1: Photolithography

During this step a pattern is transferred to the photoresist material, which is deposited as a layer on the wafer, using UV light filtered through a mask. The mask is fabricated on a glass substrate with a chromium layer on one side. The layout created in CoventorWare was sent to the mask makers where it was used to pattern the chromium with ion beam lithography. The steps involved in photolithography include spin-coating the resist, soft bake, exposure, development,

and hard bake. The parameters for each of these steps were fine-tuned to obtain the optimal recipe for photolithography.

The photoresist used for this process is AZ9260 which is a comparatively thick resist that is required for a mask during deep etches. In order to promote adhesion of the resist, hexamethyldisilazane (HMDS) was spun at 3000 rpm at 60 seconds. This is followed by spinning AZ 9260 at 500 rpm for 15 seconds for the initial spread and then at 2000 krpm for 60 seconds to obtain a uniform 6 μm thick layer on the wafer. After letting the wafer sit horizontally for a few minutes it is soft-baked at 110 ˚C for 3 minutes. This step ensures that solvent is driven away to prevent mask contamination or sticking to the mask during exposure, and to further improve the adhesion of the resist to the wafer. The soft bake also anneals the shear stresses introduced during the spin coating process [66, 67].

The exposure system used was the Karl Suss MA6 mask aligner. This comprises of a UV source controlled by a constant intensity controller (CIC). The exposure was performed with the mask and the wafer at hard contact; this can lead to possible mask or wafer contamination but provides the best resolution. The exposure was performed at an intensity of 12 mW/cm^2 for 40 s (480 mJ of energy). The wafer is then developed in a 1:4 dilute solution of AZ400K, a potassium based developer. The development typically takes 2 minutes during which time all the exposed photoresist is dissolved leaving the desired pattern on the resist. The wafer is then rinsed with deionized (DI) water and hard baked at a temperature of 110 ˚C. The purpose of the hard bake is to further strengthen the resist and promote adhesion by driving away any remaining moisture making the photoresist ready to be used as a mask in the etching step [67].

3.2.2: Deep Reactive Ion Etching

Reactive ion etching (RIE) is a process that combines physical and chemical etching. A plasma is generated by applying a radio frequency (RF) voltage to the gas to create reactive species that form volatile compounds with the material to be etched. At the same time, there are neutral species that attack the surface physically causing some isotropic etching. It is challenging to achieve deep vertical trenches with traditional RIE processes due to their slow etch rates and increasing difficulty to maintain anisotropy during long etch processes. Figure 3.8 shows a schematic of the major components of an RIE system.

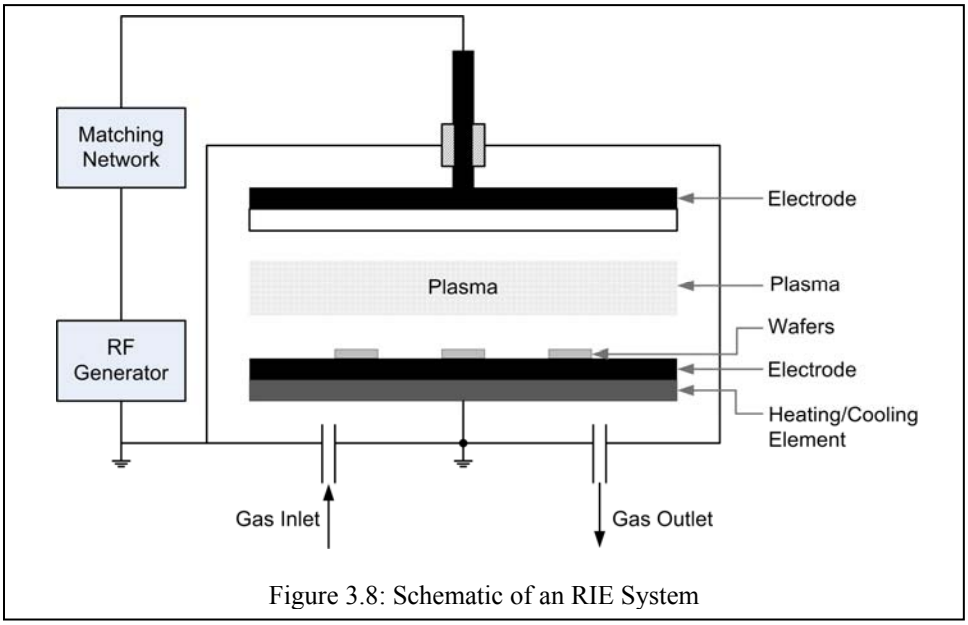

Figure 3.8: Schematic of an RIE System

New sources that produce high density of ions were made possible by the introduction of the inductively coupled plasma (ICP). In this case, the RF signal in a coil produces a time varying magnetic field which in turn generates the plasma through magnetic coupling. This solved the problem of etch rates and achieved high etch rates up to 4-6 μm/min. The DRIE process was created to accomplish a high degree of anisotropy with sidewall angles of ~1˚ or less. One way to accomplish this is by a cryogenic process where the wafer is chilled to slow down the etching on the sidewalls [68].

The process employed in the fabrication of the GC columns is the Bosch process which uses alternating etching and passivation steps. A polymer deposited on the wafer during the passivation step protects the sidewalls in the etch step where the flat surfaces are more susceptible to etching. This is explained graphically in Figure 3.9 where an isotropic etch is completed [Figure 3.9(b)] followed by a passivation step [Figure 3.9(c)]. In the next etching step the polymer on the sidewalls is protected while another isotropic well is created [Figure 3.9(d)]. This process inherently results in some scalloping effect on the sidewalls but the overall surface remains fairly planar with roughness of about 50nm [69] as seen in the SEM image of Figure 3.10.

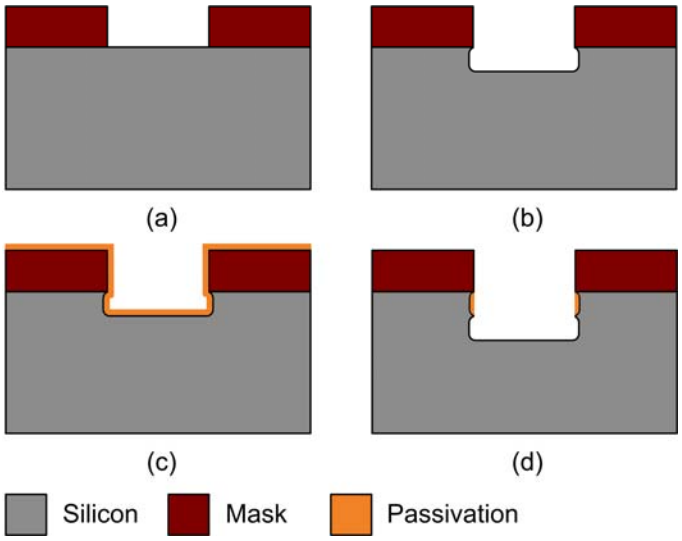

Figure 3.9: Etching and passivation steps in the Bosch process

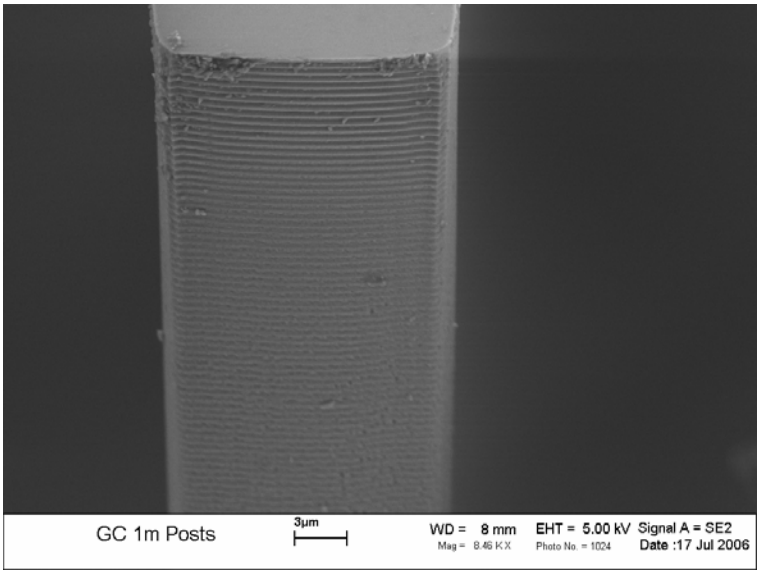

Figure 3.10: SEM image of a post in a semi-packed channel demonstrating the scalloping effect of the Bosch process

The recipe used Sulfur hexafluoride (SF_6) as the etchant for silicon and Octafluorocyclobutane (C_4F_8) as the passivation layer which is a Teflon like polymer. The etch recipe needed to be optimized with the goal being to obtain near vertical sidewalls with planar surfaces and a fast etch rate. Figure 3.11 shows the SEM images of some of the attempts at the etching process which resulted in negative sidewall angles (top-left), damaged tops of channels (top-right), overetching (bottom-left), and the result of the final recipe (bottom-right) which is

summarized in Table 3.2. The source generator is the RF generator which results in the plasma formation while the substrate-holder (SH) generator is a low-frequency (LF) generator at which the wafer is biased.

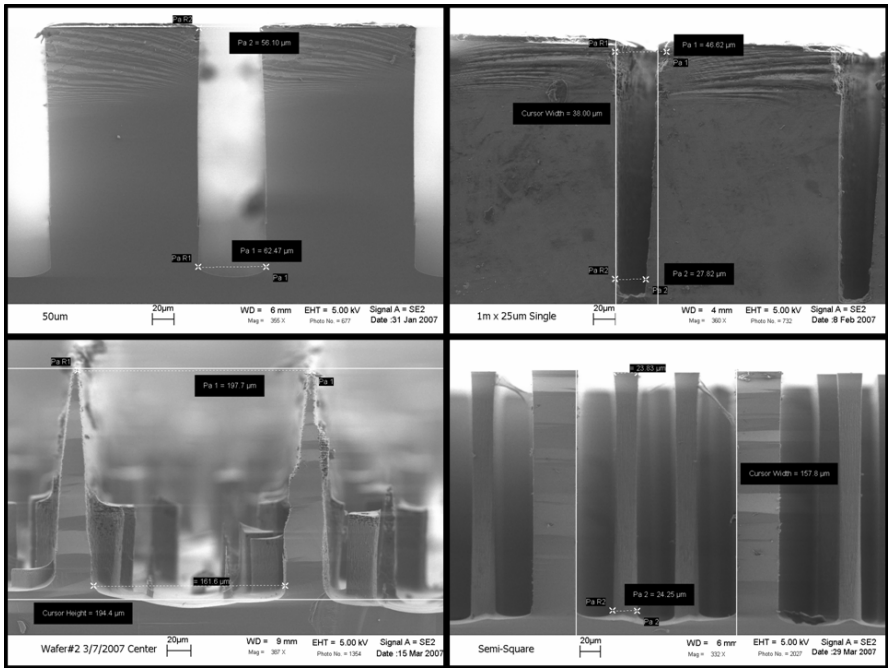

Figure 3.11: SEM images of recipes during the optimization process with the final result at bottom-right

Table 3.2: Parameters used in the final etching recipe

Gas			
Pulsed	Inactive State (sccm)	Active State (sccm)	Duration (s)
SF6	0	300	7
C4F8	0	150	2.5
Power/Pressure			
Gas	Pressure (mbar)	Source Generator (W)	
SF6	0.045	1800	
C4F8	0.045	1800	
Substrate Holder (SH) Generator			
	Power (W)	Duration (ms)	
High	60	20	
Low	0	80	
Center He Pressure: 10 mbar			
SH Position: 200 mm			
SH Temperature: 0˚C			

The important parameters that needed to be fine tuned were the chamber pressure and the duration of the etching and passivation times. These determine the anisotropy of the etch since the passivation layer protects the sidewalls and the pressure determines the randomness in the path of the species. The temperature of the substrate holder (SH) is also an important parameter as this will directly affect the rate of the reaction at the wafer. This recipe resulted in an etch rate of about 4 µm/min which made it possible to achieve the desired 240 µm depths in an hour.

After etching, the remaining photoresist is stripped with acetone and the wafer is cleaned in the DRIE system with oxygen plasma for 10 minutes (200 sccm, 0.08 mbar, 20 ˚C) followed by a piranha clean for 10 minutes (equal parts 96% H_2SO_4 and 30% H_2O_2). The plasma and piranha clean ensure the complete removal of the remaining polymer from the resist and provides a clean surface for anodic bonding. Figure 3.12 shows SEM images of etched semi-packed columns for the three generations of design.

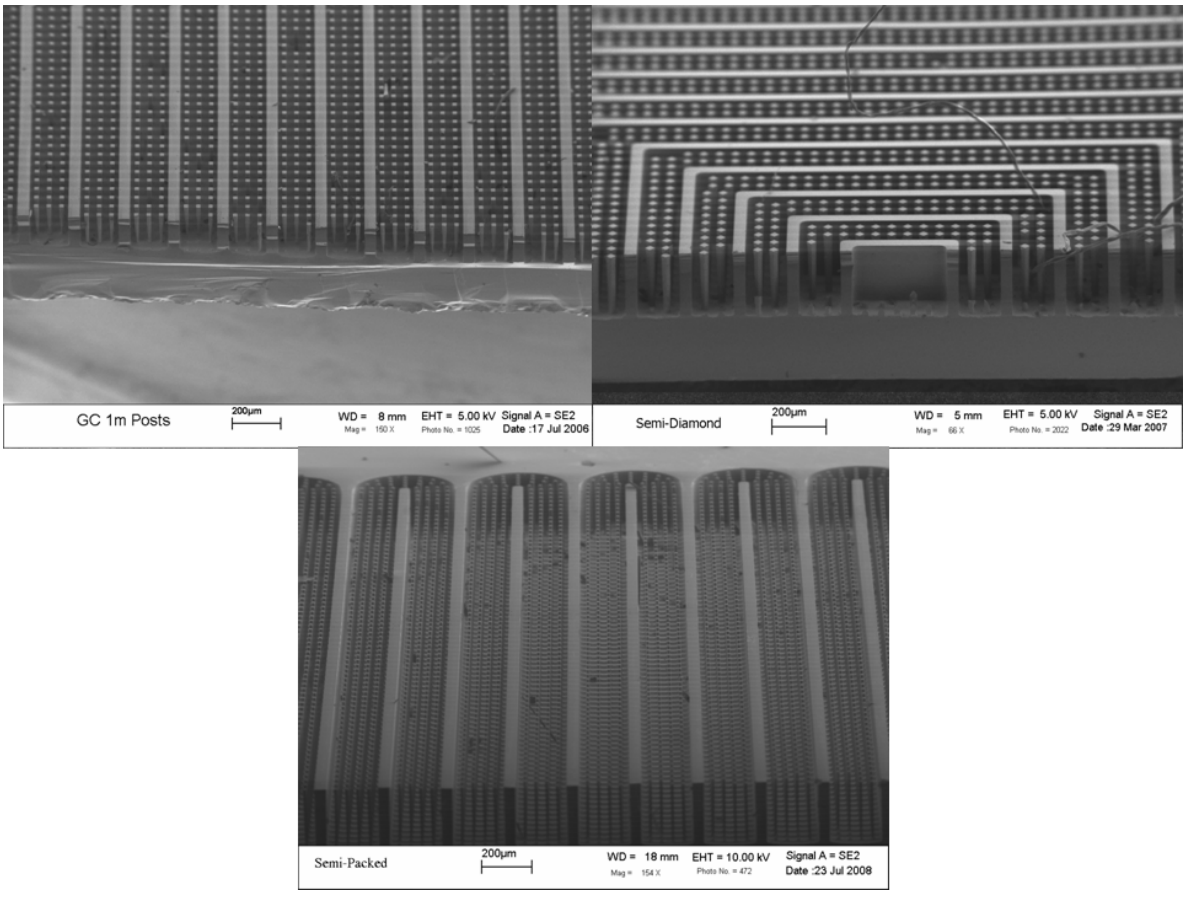

Figure 3.12: SEM images of sections of 1st generation (top-left), 2nd generation (top-right), and 3rd generation (bottom) etched semi-packed columns

3.2.3: Anodic Bonding

The third main step in the process is anodic bonding during which a Pyrex wafer is bonded to the etched silicon wafer. This is brought about by bringing the wafers in intimate contact by applying pressure under a high electric field and at a high temperature [70]. The pressure is applied by an aluminum weight which also acts like a cathode whereas the hot plate acts as the anode. Figure 3.13 shows the setup for the anodic bonding process.

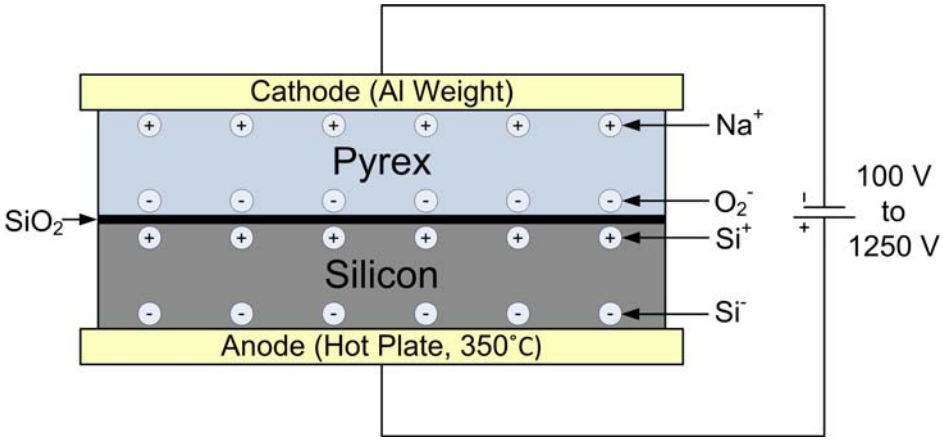

Figure 3.13: Anodic bonding setup

The high temperature of 350 ˚C makes the ions in the glass mobile while the electric field creates charged regions in the wafers. At the silicon-glass interface, Si^{+} ions and the $O2^{-}$ ions form a thin layer of SiO2 with a thickness of ~20 nm forming a hermetic seal of the channels [71, 72] as demonstrated by the SEM images of Figure 3.14.

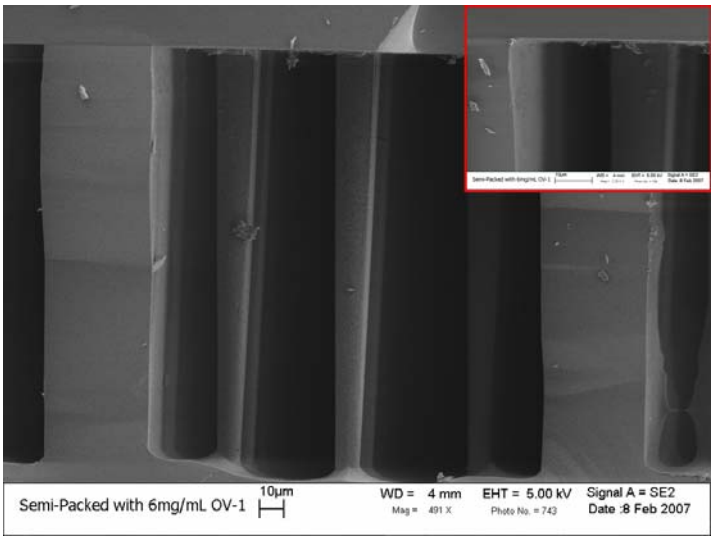

Figure 3.14: SEM images of the silicon glass interface demonstrating the integrity of the seal

3.2.4: Packaging

After anodic bonding, the wafers are diced to form the chip sized columns. A MicroAutomation MA-1006 dicing saw employed a 45 μm diamond grit saw which would make a cut of ~300 μm in width. DI water is used as lubricant to keep the saw and substrate cool. The channels are automatically opened at the microfluidic ports as the result of the dicing. This caused the dicing debris to flow into the channel along with the DI water flow which would then become lodged in the channel. In the later generations, 400 μm of spacing was provided in between each die to prevent this. The ports were later opened using an etch pen with care taken that the channels remain clean.

The chips are then attached to 100 μm ID deactivated fused silica tubing approximately 30 cm in length on each port. Epoxy, with a ceiling temperature of 250 ˚C, was used to seal the connection at the port opening. Both commercially deactivated and in-house deactivation was used. The process and significance of deactivation is described in the next section. Figure 3.15 shows the pictures of 1st generation and 3rd generation 1 m-long semi-packed columns.

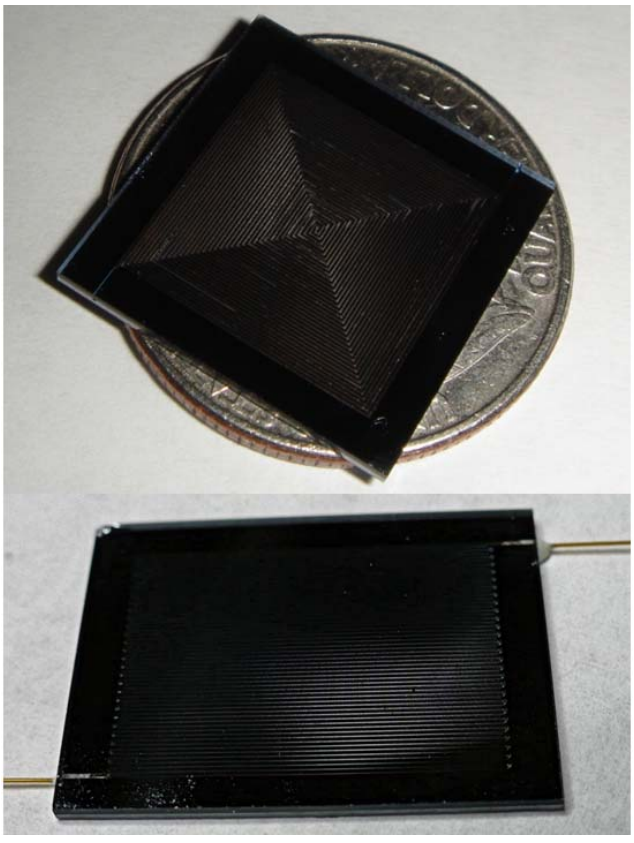

Figure 3.15: 1st generation semi-packed column after dicing and 3rd generation semi-packed column after being attached to the tubing

3.3: Coating Procedure

There are two main conventional methods of coating, dynamic and static. Dynamic coating involves pushing a plug of the stationary phase solution through the column with the help of a non-reactive gas. After the plug exits the column the excess solvent is removed by continuous gas flow. The thickness of the coating depends on the velocity and concentration stationary phase plug. Static coating involves filling a column with a stationary phase and sealing one end while a vacuum is applied to the other end. This results in the slow evaporation of the solvent leaving behind the stationary phase. The static method is generally preferred for coating purposes and is used to coat the MEMS columns as it results in a more uniform coating and the thickness is easier to calculate as it does not involve plug velocity [24]. It is first necessary to deactivate the tubing before coating the column which is explained in the next section.

3.3.1: Deactivation

Active sites on the surface of the column decrease coating performance as they interact with the analyte as it travels through the column. These sites are very common on the fused silica tubing in the form of silanol groups (Si-OH). Silanol can also attract moisture on the surface through hydrogen bonding which is detrimental to the column performance. It is therefore necessary to treat the tubing to remove these groups and make the surface inactive. Octamethylcyclotetrasiloxane (D4) has been reported as an effective deactivation agent that forms stable bonds with the surface of the tubing [73]. The D4 ring can open up at high temperatures and the terminal hydroxyl or the tetrasiloxane will interact with the silanols forming stable Si-O-Si bonds by eliminating water in the process. Figure 3.16 shows the fused silica surface and the D4 ring before and after its breakdown.

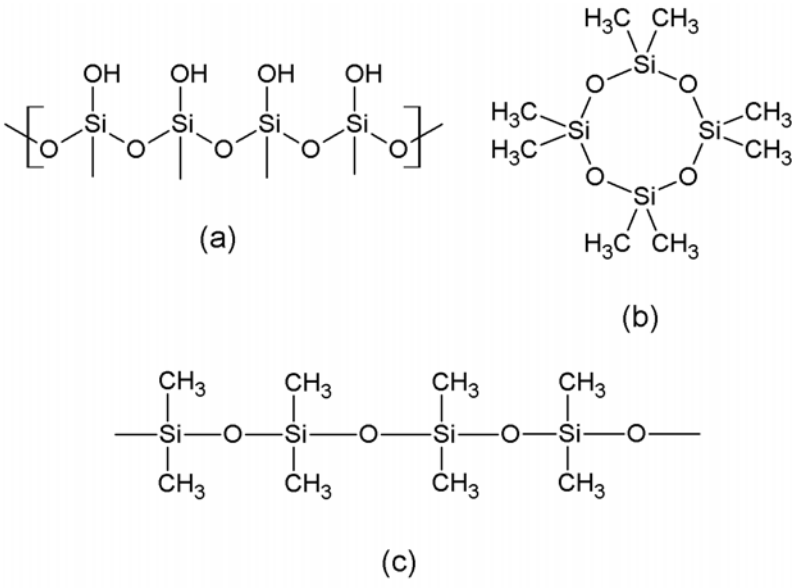

Figure 3.16: (a) Surface of the fused silica, (b) D4 in its cyclic form, and (c) after breakdown at 400 ˚C

The tubing was partially filled with D4 and sealed at both ends to be kept in the oven at 400 ˚C for 90 minutes for deactivation. Then, the tubing was washed with 0.5 mL of methylene chloride and then purged with helium at 220 °C for 60 minutes to remove all the water and the remaining D4. Even though the silicon surface should be inactive with the native oxide layer, the deactivation procedure was repeated after connecting the tubing to the MEMS columns to deactivate the chip to ensure that Pyrex surface is free of active sites. Due to the temperature limitations of the epoxy, the chip deactivation was performed at 250 °C for 90 minutes. The washing and purging procedures were also repeated.

3.3.2: Coating

The column was coated with Polydimethylsiloxane (PDMS), a popular silicone based coating polymer, using static coating procedures as published in [24]. A solution of PDMS dissolved in n-pentane with a known concentration was used to fill the column and one end of the column was sealed by pushing a small amount of wax into the capillary tubing. A vacuum was then applied to the other end while the column was kept in a water bath maintained at a temperature of 35 °C. This resulted in slow evaporation of the solvent, leaving behind a thin layer of stationary phase coating on the walls. The vacuum was continued until a final pressure of 0.2 mTorr was reached in the column to ensure the complete evaporation of the solvent. In order to

obtain a stable film, the PDMS was cross-linked by passing the vapor of azo-tert-butane (ATB) over the stationary phase for 60 minutes as shown by the following reaction [73, 74].

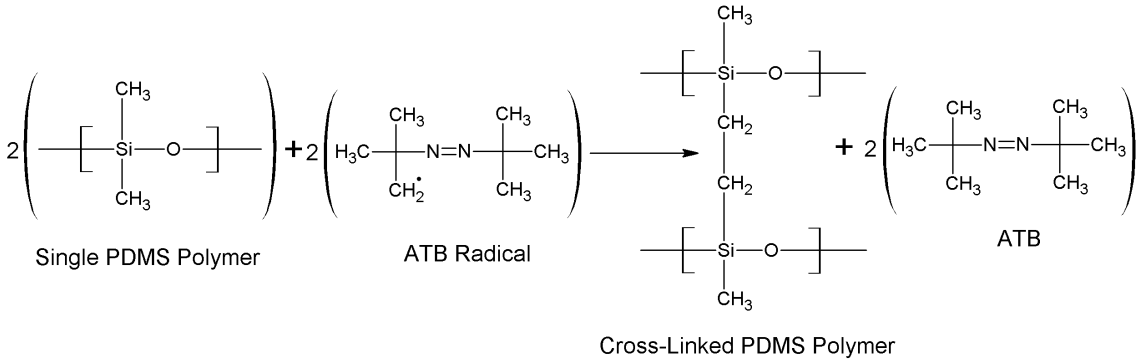

Figure 3.17: Cross-linking of PDMS with the ATB free radical

Finally, the column was sealed at both ends and heated at 220 ˚C for 60 minutes to cure the stationary phase. SEM images of the coated channels show a thicker coating layer at the corners and also demonstrate the pooling effect at the end of the semi-packed posts. The coating increases from ~400 nm at the middle of a channel to almost 1.5 μm at the corners which is an undesirable effect but is unavoidable with traditional coating methods.

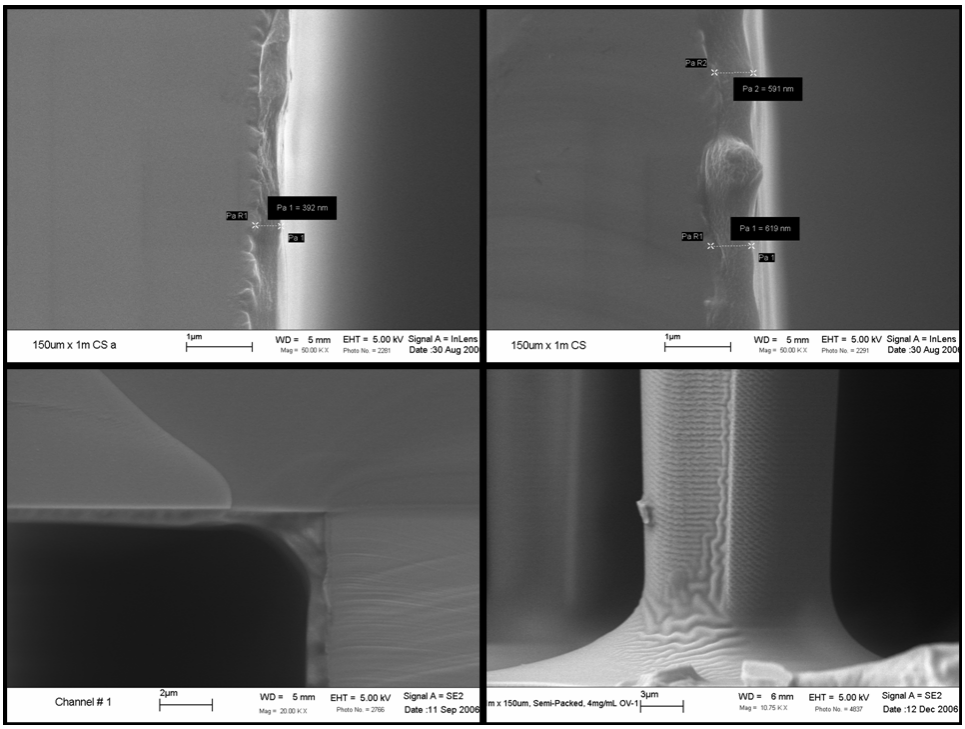

Figure 3.18: SEM images of coating. Clockwise from top-left: middle of the column wall, closer to a corner, bottom of a post, and corner of silicon-glass interface.

CHAPTER 4: Results and Discussion

The performance of a GC column can be measured in several ways, a few of which are mentioned in section 2.4. The selection of a GC column involves tradeoffs between sample capacity, resolution, speed, and sensitivity. It is the goal of the semi-packed design to minimize these limitations and create a column layout that has advantages in all areas. The main criteria for determining the performance of the column is considered to be the separation efficiency defined by the theoretical plates. Columns with high efficiency can separate larger number of compounds and also achieve faster separation times without sacrificing the resolution of the separation as they have lower band broadening.

Another figure of merit explored in this study is the sample capacity of the column. This is particularly significant for μGC systems operating in the field where the samples cannot be prepared to match both the detector's sensitivity and the column's capacity. The sample capacity can be enhanced by increasing the thickness of the stationary phase or the surface area of the column wall. In conventional columns, both these methods cause a drop in efficiency. In MEMS columns, however, the surface area can be increased without affecting the efficiency as there are two degrees of control, width and height, for the dimensions of the columns.

Most of the testing on the OV-1 coated columns was performed within a week of coating. This was due to the fact that the coating on the MEMS columns was unstable and would wear off in a few days time. Though the results were reproducible from column to column, each column itself was not able to reproduce the results after a few days. The columns would still work but the performance quality would reduce over time.

4.1: Experimental Setup

As the MEMS columns were not yet integrated with other GC components, the chips were tested with a conventional GC system to which they were attached via the fused silica tubing. An HP5890 GC (pictured in Figure 1.1) was used as the oven for temperature programming. The injection port of the oven was maintained at 280 ˚C to instantly vaporize the sample and was

attached to an HP7673 autosampler. The autosampler is capable of high speed injections for very narrow initial plug widths minimizing the *D*-term (see section 2.3.4).

The samples were detected using a flame ionization detector (FID) which was also maintained at 280 ˚C. This detector uses air and hydrogen to maintain a jet of flame that ionizes the sample as it passes through. The electrons are then propelled towards a collector by an electric field and the current is amplified and converted to a voltage signal by an electrometer [46]. The signal is then fed into a data acquisition system. The hydrogen is supplied by a generator that uses DI water to generate the gas and a pressurized industrial gas tank was used for the air supply. Due to its inertness, helium was used as the carrier gas which was also supplied by a gas tank.

The data acquisition system sampled the FID signal at a rate of 20 Hz and converted it to a digital signal for the computer. HP ChemStation software was used to control all the components of the GC system and to analyze the generated chromatograms.

After the completion of the coating, the columns were first conditioned at a temperature of 200 ˚C for an hour in the GC oven while maintaining a carrier gas flow. This was to remove any external residue that may have entered the column before it was installed in the GC oven and the carrier gas flow was started.

4.2: Separations

To test the performance of the coating, the columns are first tested with an eight component industry standard mixture that contains polar and non-polar components. Tailing in the peaks of the polar components indicates the presence of any active sites on the peak while the heights of the non-polar peaks characterize the retention of the stationary phase. These components are listed in Table 4.1 in the order of their elution times along with their primary function and boiling points.

Table 4.1: Components in the standard mixture with their boiling points and purpose

Elution Order	Component	Boiling Point	Purpose
1	2-Octanone	173	Lewis acid sites
2	1-Decane	174	Retention
3	1-Octanol	195	Hydrogen bonding sites
4	2,6-Dimethyl Phenol	201	Basic active sites
5	Undecane	196	Retention
6	2,6-Dimethyl Aniline	214	Acidic active sites
7	Dodecane	216	Retention
8	Tridecane	234	Retention

1 μL of the mixture dissolved in methylene chloride (CH_2Cl_2) was injected into the columns at 35 ˚C and the temperature was ramped to 140 ˚C at 10 ˚C/min. The components were separated with sufficient resolution in under three minutes as seen in the chromatogram below. There is some amount of tailing in the active components which indicate that the column wasn't completely deactivated. It is possible that the Pyrex and the silicon surfaces also contain active sites and the deactivation at the reduced temperature of 250 ˚C (as opposed to the standard 400 ˚C) may not have completely removed these sites. The equal height of the non-polar components shows that the retention quality of the stationary phase is good.

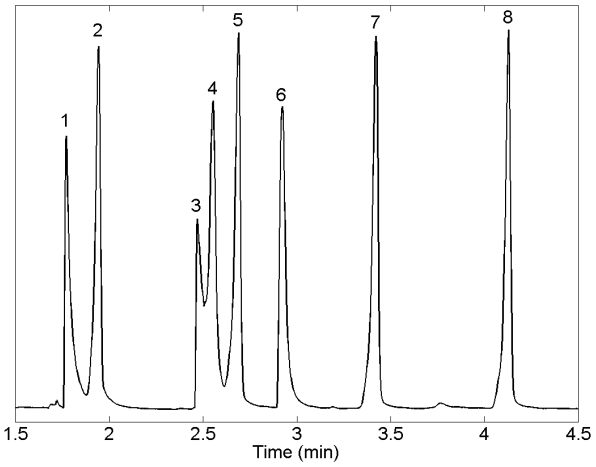

Column: 1 m 1st generation semi-packed column

Coating: 6 mg/mL OV-1

Temp.: 35-140 ˚C @ 30 ˚C/min

Figure 4.1: Chromatogram showing the separation of the eight component mixture obtained by a 1st generation semi-packed column

The temperature ramp can be increased in order to achieve faster analysis times but at the cost of sacrificing the resolution of the separation. The following chromatogram shows the separation of seven straight chained alkanes at rates of 10 ˚C/min and 30 ˚C/min.

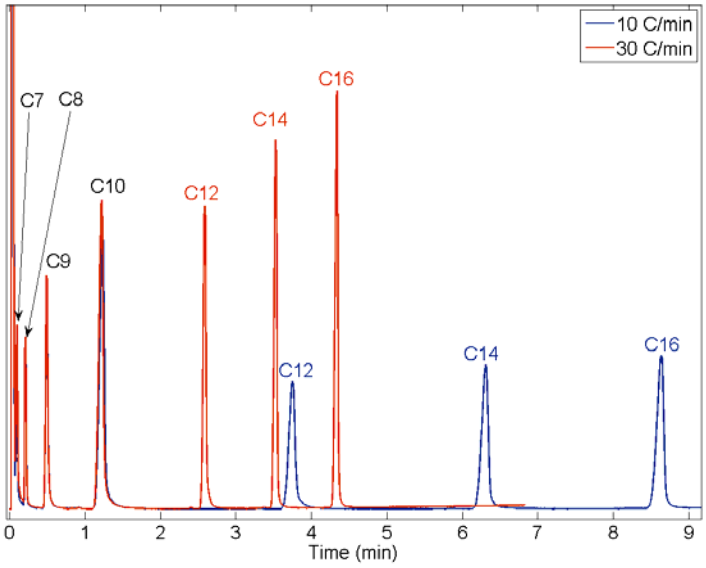

Column: 25 cm 2nd generation semi-packed

Coating: 4 mg/mL OV-1

Temp.: 35-140 ˚C @ 10 and 30 ˚C/min

Figure 4.2: Separation of alkanes at two temperatrure ramps with 2nd generation square

This separation was achieved with the second generation semi-packed design with square posts. The separation time has been halved by increasing the temperature ramp and, in this case, there is no loss of resolution indicating that the ramp can be increased further. This, however, was not possible with the conventional GC oven that had reached its temperature ramping limits. The MEMS columns can be integrated with on-chip heaters and other sensors which can achieve a ramp rate up to hundreds of degrees per second. Figure 4.3 shows the back of 25 cm-long column on which heaters and a temperature sensor have been deposited by evaporating Pt/Ti on a patterned mask which is later removed leaving the metal in the desired pattern.

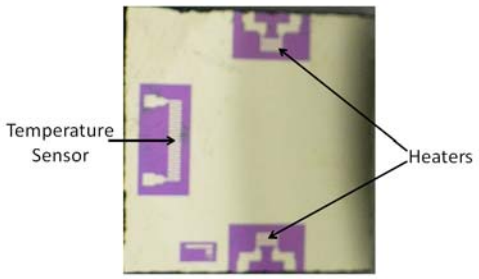

Figure 4.3: Backside of a column with the Pt/Ti heaters and temperature sensor

The same mixture of alkanes was also separated using an open column based on the second generation design seen in the chromatogram in Figure 4.4 along with the separation achieved by the semi-packed channel with the square posts. The temperature programming for the separations was 35-140 ˚C at 30 ˚C/min.

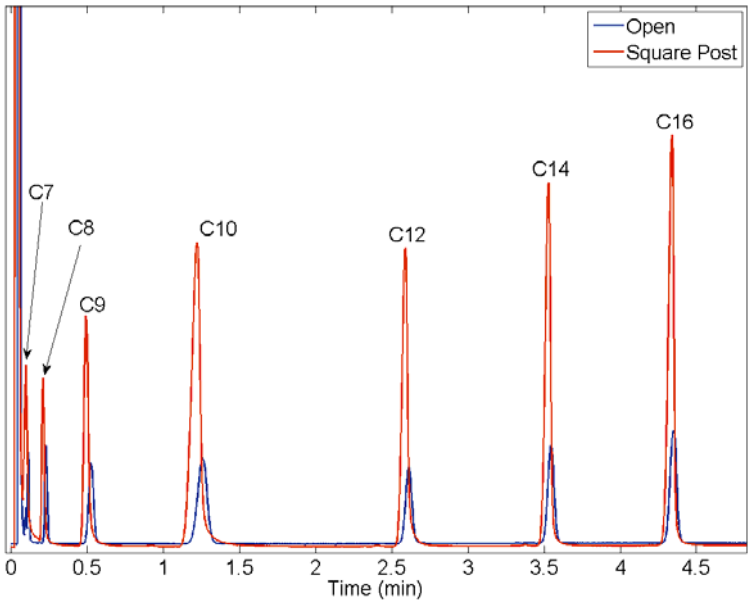

Column: 25 cm 2nd generation semi-packed and open rectangular

Coating: 4 mg/mL OV-1

Temp.: 35-140 ˚C @ 30 ˚C/min

Figure 4.4: Separation of alkanes with 2nd generation open and semi-packed designs

The effects of overloading are seen in the peaks of the separation with the open column which show an asymmetrical leading effect causing a drop in the separation efficiency. The semi-packed column yielded symmetrical peaks without the leading effect demonstrating their higher sample capacity.

4.3: HETP Measurement

The HETP was experimentally calculated using nonane (C_9H_{20}) and methane (CH_4). The width and height of the nonane peak were used in Equation 2.1 to get the plate number and the methane peak to calculate the average linear carrier gas velocity ($\bar{u}$). The minimum HETP is independent of the retention factor (see section 2.1) after a value above 10. Nonane has a retention factor for >20 under all testing pressures and hence was chosen for the measurement of the HETP which was calculated from the plate number using Equation 2.2. A small quantity of nonane and methane was sealed in a vial and 1 µL of the vapor in the vial was injected into the column at 28 ˚C. Due to the low sampling rate of the data acquisition system (20 Hz) the data points were insufficient to accurately measure the peak's retention time and width. This was fixed by plotting the data files in MATLAB and fitting them to a Gaussian profile in order to obtain the proper retention time and half height width. Figure 4.5 shows a chromatogram peak

with the methane and nonane peak and the Gaussian profile fitted to the latter. Each injection was repeated three times to ensure the linear velocity, retention time and width measurements are accurate.

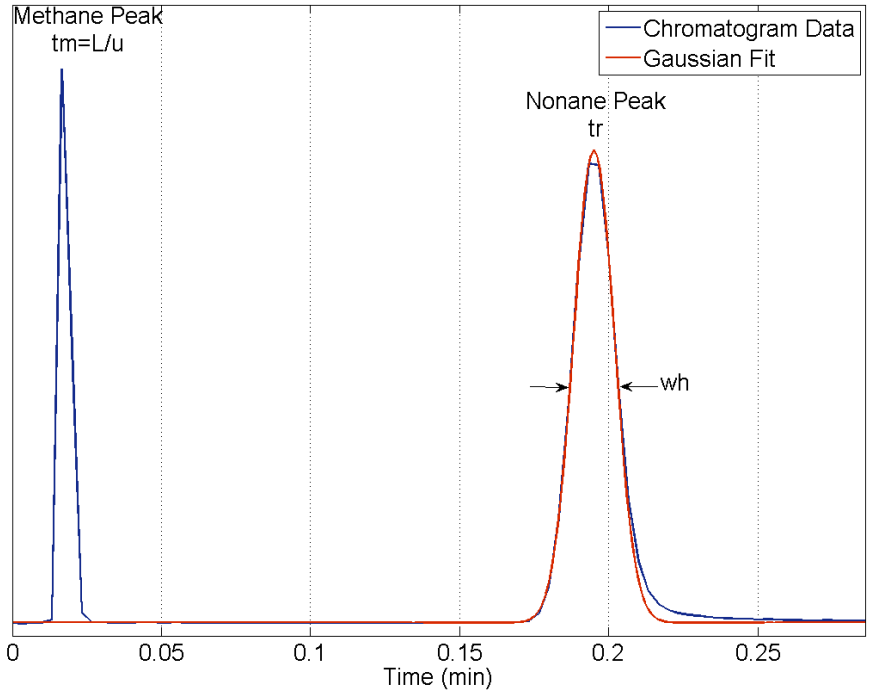

Figure 4.5: Chromatogram used to plot the HETP points for efficiency calculation

4.3.1: First Generation Columns

The 1st generation open and semi-packed columns were coated with a 6 mg/mL solution of PDMS. The coating thichness (d_f) based on the volume and surface area of the channels was calculated to be 0.25 µm and 0.1 µm, respectively, for the open rectangular and the semi-packed columns assuming a uniform coating. However, as seen in the SEM images, the coating is not very uniform and is thicker at certain places. The following figure shows the HETP calculations for both the columns. The calculated data points were fitted to Equation 2.3 to obtain the curves. It is seen that the semi-packed column shows a two-fold improvement in the separation efficiency with an HETP of 0.01 cm (10,000 plates/m) as compared to an open rectangular MEMS column having the same outer dimensions.

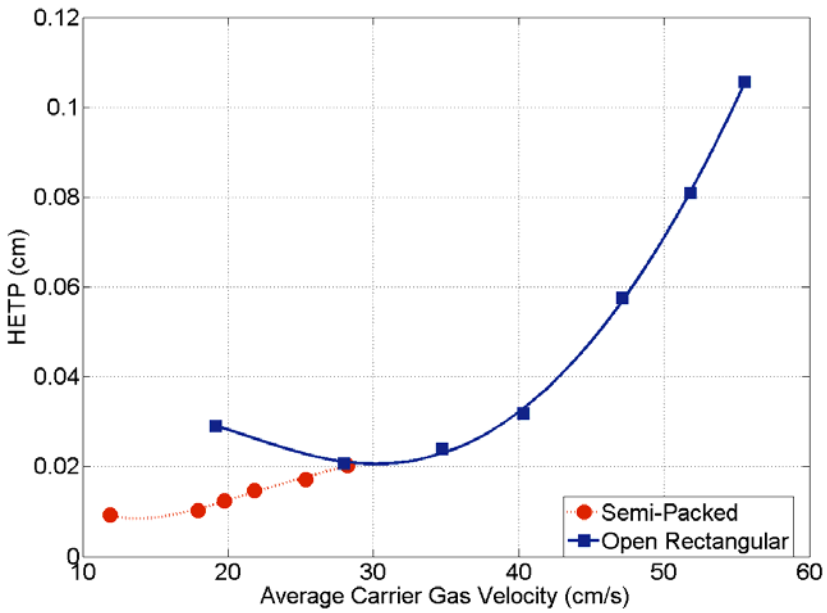

Figure 4.6: HETP plotted for the 1st generation open and semi-packed columns

The increase in efficiency observed in semi-packed columns cannot be attributed only to the reduction in their effective width as compared to an open rectangular MEMS column. The effective width of the semi-packed column is about 126 µm. This only amounts to a 20% decrease in the width. The decrease in the stationary phase thickness also cannot account completely for the improvement in efficiency as studies have shown that decreasing the thickness from 0.25 µm to 0.10 µm increased the efficiency only by about 25% [75]. It should also be noted that the semi-packed column, having more corners in its geometry, will have more areas where the stationary phase has pooled and become thicker as compared to the open-rectangular columns. Furthermore, the mass transfer in the stationary phase (C_S) is proportional to the thickness of the stationary phase whereas, the mass transfer in the mobile phase (C_M) is proportional to the dimensions of the column. In columns with larger dimensions compared to the thickness of the stationary phase, as in this case, C_M becomes the main contributor to band broadening as compared to C_S. Hence, the thickness of the stationary phase (d_f) becomes less significant compared to the geometry of the column. Figure 4.7 shows the velocity profiles of the two channel configurations at their optimal velocities of 12 cm/s and 28 cm/s for the semi-packed and the open rectangular columns with pressure drop of 2.39 psi/m and 0.373 psi/m respectively.

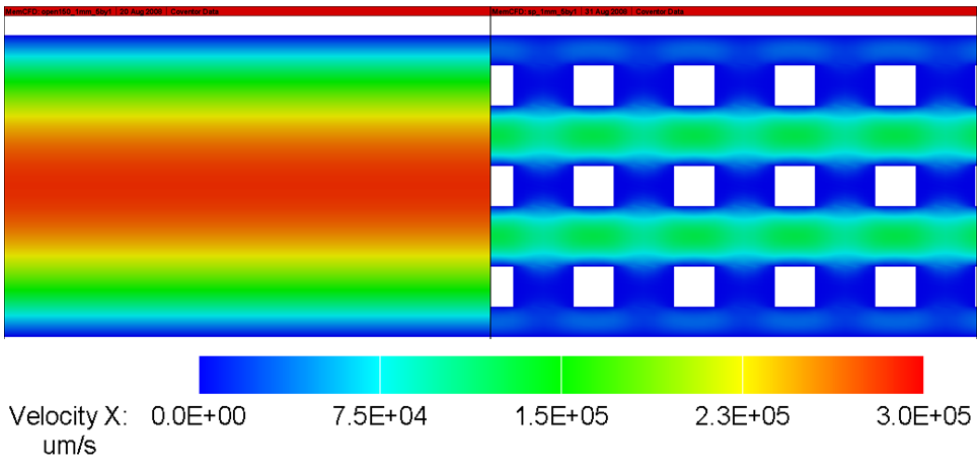

Figure 4.7: Velocity profile for the 1st generation channels simulated at their optimum velocities

In spite of the higher pressure drop, it is believed that the major contributor to the separation efficiency enhancement in semi-packed columns is that the posts modify the velocity profile of the column to minimize the broadening. The other main contributor is the shorter mass transfer distances in the mobile phase in the semi-packed column. These factors ensure that the original plug of sample introduced into the column experiences less band broadening.

4.3.2: Second Generation Columns

The 2nd generation columns, due to their shorter lengths, were coated with 4 mg/mL of PDMS as opposed to 6 mg/mL. The coating thickness with this concentration is 0.2 µm for the open rectangular columns and 0.07 µm for the square semi-packed columns. The coating of the diamond and long posts designs was unsuccessful due to blockages during the cross-linking process. This may be because of the narrow regions being longer in the long-post designs and minimum gap being narrower in the diamond-post designs. The HETP was measured in the same way as previously mentioned. In this case, though the semi-packed column showed a better efficiency, the difference was not significant. This may be due to the fact that the column length was only 25 cm while the total length of the tubing was 35 cm. The effect of the geometry of the column was not a major contributing factor in the efficiency of the system. Figure 4.8 shows the HETP measured for the open and square post semi-packed channels along with their velocity profile simulations at optimum conditions.

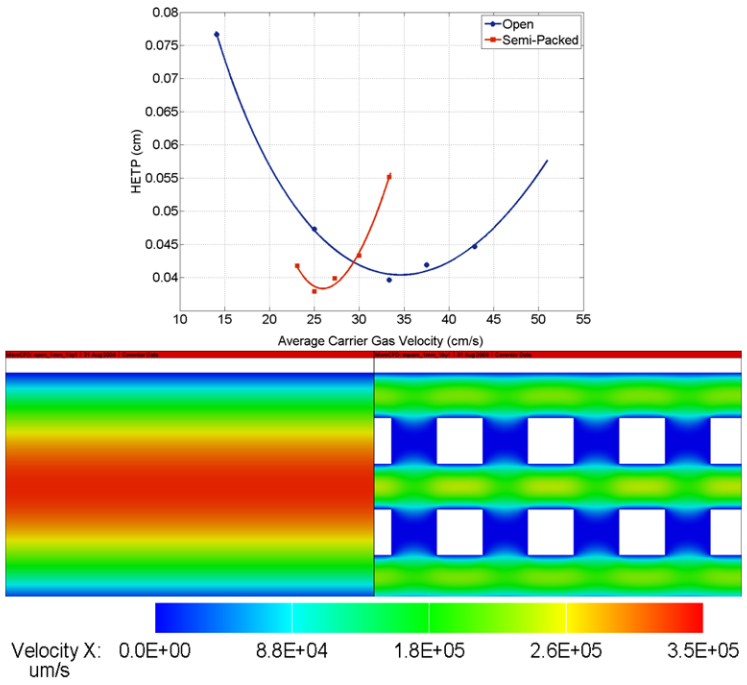

Figure 4.8: HEPT for 2nd generation open and square semi-packed channels with optimal velocity profiles

4.3.3: Third Generation Design

In the 3rd generation design it was decided to shift back to 1 m-long columns as the 2nd generation geometries did not reveal any significant differences. A major change in the efficiency calculation of these columns was that they were tested without any coating using methane for both, linear velocity and plate number calculation. This cannot be translated to the HETP as defined but still gives an idea of the effects of column geometry on the variance of the peak; this is still a good measure of efficiency. All other conditions in the efficiency calculations were kept the same. The following Table 4.2 summarizes the results of all the 3rd generation designs (see Table 3.1). It is seen that the semi-packed columns still give a better performance even though some of them have a higher effective width. The effective width of the SP1 design is comparable to the width of OR120 and yet the SP1 configuration yields a slightly higher plate number. However, the OR90 design has a higher efficiency than the SP1 design with the same minimum diameter. Among the semi-packed designs themselves, there is a direct correlation between the pressure drop and efficiency; that is, the efficiency increases with decrease in pressure drop regardless of the increase effective diameter. This trend may reverse once the effective diameter reaches a certain upper limit where the effects of pressure drop become less

significant compared to the large mass transfer distances as is the case in the open rectangular channels. This shows that the enhanced efficiency of the semi-packed design is due to the combined result of effective diameter, mass transfer differences and pressure drops.

Table 4.2: Summary of results in the 3rd generation columns

	N	$\bar{u}$ (cm/s)	P (psi/m)	Effective Width
OR90	2500±3%	30.2	0.834	90
OR120	2000±2%	27.7	0.432	120
SP1	2200±2%	22.5	0.576	126
SP2	2350±3%	29.0	0.531	134
SP3	2400±2%	29.7	0.751	158
SP4	2550±3%	27.7	0.506	169

The semi-packed channels also provide configurations with lower velocity variation which further reduces band broadening as seen in the simulation in Figure 4.9. The lower optimal velocity generally seen in the semi-packed design may result in slower analysis times but this can be resolved by increasing the temperature ramps without loss in resolution due to their high separation efficiency.

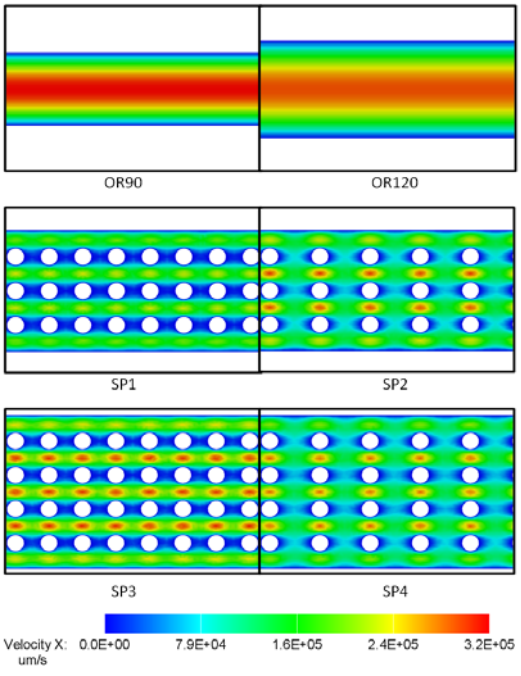

Figure 4.9: Velocity profiles of 3rd generation channels at optimal

4.4: Sample Capacity

As mentioned earlier, in addition to providing higher separation efficiencies, the semi-packed columns have a larger sample capacity by virtue of their larger surface areas. The sample capacity is directly proportional to the amount of stationary phase which in turn is a product of surface area and thickness of the stationary phase. Increasing the thickness causes a drop in the separation efficiency. In the case of open columns, increasing surface area increases the mass transfer distances though this effect can be limited in rectangular columns by keeping one dimension small. The semi-packed columns have a large surface area while at the same time they provide lower mass transfer distances.

To test the sample capacity of the columns solutions of dodecane ($C_{12}H_{26}$) in methylene chloride (CH_2Cl_2) were prepared in increasing concentrations from 250 ng/µL to 10 µg/µL. The solution was injected in to the coated columns at 75 ˚C and at a split ratio of 200:1, i.e. only a 200^{th} fraction of the total injected volume is directed into the column. Dodecane was chosen because of its higher retention time which means that the solvent peak does not interfere with the analyte peak. As the concentration of the analyte increases, it reaches a point where the stationary phase gets saturated and becomes unable to adsorb the molecules to maintain equilibrium. This causes a leading effect in the peak and leads to a drop in efficiency. The coated 1^{st} generation columns were used to test the sample capacity with injections at different volumes and the following table lists the drop in the efficiency as the sample amount is increased. To demonstrate the statistical significance of the data the *t*-test was performed as described in [76]. For the chosen samples the value of *t* needs to be greater than 2.776 for a confidence of at least 95% in the measurements. It is seen that at the maximum amount of 30 µg the magnitude of *t* is much higher at 8.6 showing that the difference between the two columns is statistically significant. This is not the case with the 10 and 20 µg sample size as neither column is significantly overloaded.

Table 4.3: Effects of increasing analyte amounts on the efficiency of the column

Injection Volume (µL)	Injection Amount (µg)	Percentage Reduction in Efficiency		t
		OR	SP	
1	0.25-10	6.6±1	5.5±1	1.4
2	0.5-20	15±2	14±2	0.87
3	0.75-30	37±4	23±4	8.6

CHAPTER 5: Conclusion

The semi-packed columns have proven to be a versatile tool in the enhancement of μGC columns by providing unique geometries due to the presence of the microposts. μGC systems have special needs due to their small size. It is advantageous to minimize the size of the chip to keep costs low and yields high by maximizing the number of devices on each wafer. This puts a limitation on the length and width of channel which in turn affects the efficiency. Another challenge in the design of these systems is that μGC systems would have to be driven by micro pumps unlike conventional GC systems which are driven by industrial pressurized gas tanks. This will put some critical restraints on the pressure drops generated in the channels making it difficult to use vary narrow channels that have high efficiency but high pressure drops as well. Additionally, as μGC will be operating in the field, it will not be easy to prepare samples in the appropriate concentrations to match both the column's capacity and the detector's sensitivity. The semi-packed columns provide more versatility in the column design and thus relieving the constraints on the design of the other components of a μGC system.

When it comes to column geometry, open columns have only one parameter that can be manipulated, radius in the case of conventional columns and width for open rectangular MEMS columns. Decreasing the width causes an increase in efficiency but limits the sample capacity and results in higher pressure drops. Taking advantage of MEMS technology, semi-packed columns offer several new parameters of the posts that can be tailored to provide the optimum configuration in terms of efficiency, sample capacity, and pressure drop to meet the needs of any μGC system.

The shape, size, and spacing of the posts along with the total width of the channel can be used to attain higher efficiencies than open channels while offering a larger sample capacity. Compared to packed channels, semi-packed channels have lower pressure drops and a more uniform velocity profile. These channels are an ideal hybrid configuration that combine the advantages of open (both narrow and wide), packed, and multicapillary channels.

The semi-packed columns were tested under several conditions and compared to open columns and proved to be superior in both efficiency and sample capacity. The first generation of

semi-packed channels, coated with PDMS, provided an efficiency of 10,000 plates/m which is the highest reported to date among the MEMS columns with similar outer dimensions. It is possible to reach even higher efficiencies by optimizing the post configuration by creating a model for this new class of MEMS based μGC columns.

5.1: Future Work

In order to create a complete model for the semi-packed columns, the study on the 3rd generation columns can be expanded to incorporate a wider range of variables. In the case of the 150 μm or the 190 μm semi-packed designs, the post spacing along the length of the channel can be increased, causing an increase in the effective diameter, until a drop in efficiency is seen. This would give the optimum post spacing along the length of the channel for the particular configuration. Similarly, the change in the number of posts (SP1 to SP3 or SP2 to SP4) can also be varied to study the effects on the efficiency. The third parameter is the spacing across the width of the channel. This was kept constant for all designs in the 3rd generation columns but can be varied along with the other parameters. Once the optimum configuration is reached, a model can be created and a new expression for the HETP of these semi-packed channels can be defined. This model would be for a particular post shape but several post shapes can be compared in a study similar to the 2nd generation design and the model for the best shape adapted to produce the μGC columns.

A significant challenge in the fabrication of the MEMS columns is the coating process. Traditional static and dynamic methods have been developed for open fused silica capillary tubing. In MEMS columns, due to their sharp corners and turns, the coating is not uniform and frequently gets blocked during the cross-linking process. This puts a severe limitation on the dimensions of the columns as was experienced while coating the 2nd generation diamond and long post channels. Another issue with the coating is its instability. The coating performance would deteriorate after some days. This made it difficult to test the columns once the coating wore off. Though the results were reproducible from column to column and each column would still show some amount of separation, the quality of the separations would reduce over time. One possible way to overcome this is to develop nano-structured stationary phases that would produce conformal and thin stationary phases for the MEMS columns. Furthermore, the

deposition technique of this type of stationary phase can also be incorporated at any step of the microfabrication process.

The integration of the MEMS columns with other components to achieve a complete lab-on-a-chip GC system is the ultimate goal of this project. The columns would have on-chip heaters and sensors for pressure, temperature, and flow. This would be integrated with on-board preconcentrators, micropumps, and detection systems. Several columns can be used in series and parallel configurations having various stationary phases suited for different kinds of compounds in tandem to separate hundreds of compounds within seconds. Integrated with signal processing components to communicate with other devices, this handheld system can be used on the field to separate and detect many components in the environment.

References

[1] M. Agah, G. R. Lambertus, R. Sacks, and K. Wise, "High-Speed MEMS-Based Gas Chromatography," *Microelectromechanical Systems, Journal of,* vol. 15, pp. 1371-1378, Oct. 2006.

[2] A. Manz, N. Graber, and H. M. Widmer, "Miniaturized Total Chemical Analysis Systems: A novel Concept for Chemical Sensing," *Sensors and Actuators B: Chemical,* vol. 1, pp. 244-248, 1990.

[3] E. B. Overton, H. P. Dharmasena, U. Ehrmann, and K. R. Carney, "Trends and Advances in Portable Analytical Instrumentation," *Field Analytical Chemistry & Technology,* vol. 1, pp. 87-92, Dec. 1996.

[4] A. Rios, A. Escarpa, M. C. Gonzalez, and A. G. Crevillen, "Challenges of Analytical Microsystems," *TrAC Trends in Analytical Chemistry,* vol. 25, pp. 467-479, May 2006.

[5] E. Verpoorte and N. F. De Rooij, "Microfluidics Meets MEMS," *Proceedings of the IEEE,* vol. 91, pp. 930-953, June 2003.

[6] W. Ramsay, "A Determination of the Amounts of Neon and Helium in Atmospheric Air," *Proceedings of the Royal Society of London. Series A, Containing Papers of a Mathematical and Physical Character (1905-1934),* vol. 76, pp. 111-114, May 1905.

[7] M. Tswett, "Adsorptionsanalyse und Chromatographische Methode: Anwendung auf die Chemie des Chlorophylls," *Berichte der Deutschen Botanischen Gesellschaft,* vol. 24, pp. 384-393, 1906.

[8] M. Tswett, "Physikalisch-Chemische Studien uber das Chlorophyll," *Berichte der Deutschen Botanischen Gesellschaft,* vol. 24, pp. 316-332, 1906.

[9] H. J. Issaq, "A Century of Separation Science," New York: Marcel Dekker, 2002.

[10] A. T. James and A. J. P. Martin, "Gas-Liquid Partition Chromatography: The Separation and Micro-Estimation of Volatile Fatty Acids from Formic Acid to Dodecanoic Acid," *Biochem. J.,* vol. 50, pp. 679-690, Mar. 1952.

[11] A. J. Martin and R. L. Synge, "A New Form of Chromatogram Employing Two Liquid Phases: A Theory of Chromatography and Application to the Micro-Determination of the Higher Monoamino-Acids in Proteins," *Biochem. J.,* vol. 35, pp. 1358-1368, Dec. 1941.

[12] E. F. Barry and R. L. Grob, *Columns for Gas Chromatography: Performance and Selection*. Hoboken: Wiley-Interscience, 2007.

[13] H. M. McNair and J. M. Miller, *Basic Gas Chromatography*. New York: Wiley-Interscsience, 1998.

[14] S. C. Terry, J. H. Jerman, and J. B. Angell, "A gas chromatographic air analyzer fabricated on a silicon wafer," *Electron Devices, IEEE Transactions on,* vol. 26, pp. 1880-1886, Dec. 1979.

[15] R. R. Reston and E. S. Kolesar, Jr., "Silicon-Micromachined Gas Ghromatography System Used to Separate and Detect Ammonia and Nitrogen Dioxide-Part I: Design, Fabrication, and Integration of the Gas Chromatography System," *Microelectromechanical Systems, Journal of,* vol. 3, pp. 134-146, Dec. 1994.

[16] E. S. Kolesar, Jr. and R. R. Reston, "Silicon-micromachined gas chromatography system used to separate and detect ammonia and nitrogen dioxide. II. Evaluation, analysis, and

theoretical modeling of the gas chromatography system," *Microelectromechanical Systems, Journal of,* vol. 3, pp. 147-154, Dec. 1994.
[17] E. S. Kolesar, Jr. and R. R. Reston, "Review and Summary of a Silicon Micromachined Gas Chromatography System," *IEEE Transactions on Components, Packaging, and Manufacturing Technology, Part B: Advanced Packaging,* vol. 21, pp. 324-328, Nov. 1998.
[18] C. M. Matzke, R. J. Kottenstette, S. A. Casalnuovo, G. C. Frye-Mason, M. L. Hudson, D. Y. Sasaki, R. P. Manginell, and C. C. Wong, "Microfabricated Silicon Gas Chromatographic Microchannels: Fabrication and Performance," in *SPIE Conference on Micromachining and Microfabrication Process Technology IV*, Santa Clara, CA, USA, Sep. 1998, pp. 262-268.
[19] G. Wiranto, M. R. Haskard, D. E. Mulcahy, D. E. Davey, and E. F. Dawes, "Microengineered Open Tubular Columns for GC Analysis," in *SPIE Conference on Electronics and Structures for MEMS*, Gold Coast, Australia, Oct. 1999, pp. 168-177.
[20] H.-s. Noh, P. J. Hesketh, and G. C. Frye-Mason, "Parylene Gas Chromatographic Column for Rapid Thermal Cycling," *Journal of Microelectromechanical Systems,* vol. 11, pp. 718-725, Dec. 2002.
[21] G. Lambertus, A. Elstro, K. Sensenig, J. Potkay, M. Agah, S. Scheuering, K. Wise, F. Dorman, and R. Sacks, "Design, Fabrication, and Evaluation of Microfabricated Columns for Gas Chromatography," *Anal. Chem.,* vol. 76, pp. 2629-2637, May 2004.
[22] C.-J. Lu, W. H. Steinecker, W.-C. Tian, M. C. Oborny, J. M. Nichols, M. Agah, J. A. Potkay, H. K. L. Chan, J. Driscoll, R. D. Sacks, K. D. Wise, S. W. Pang, and E. T. Zellers, "First-Generation Hybrid MEMS Gas Chromatograph," *Lab on a Chip,* vol. 5, pp. 1123-1131, Oct. 2005.
[23] M. Agah, J. A. Potkay, G. Lambertus, R. Sacks, and K. D. Wise, "High-performance Temperature-Programmed Microfabricated Gas Chromatography Columns," *Journal of Microelectromechanical Systems,* vol. 14, pp. 1039-1050, Oct. 2005.
[24] S. Reidy, G. Lambertus, J. Reece, and R. Sacks, "High-Performance, Static-Coated Silicon Microfabricated Columns for Gas Chromatography," *Analytical Chemistry,* vol. 78, pp. 2623-2630, April 2006.
[25] M. Agah and K. D. Wise, "Low-Mass PECVD Oxynitride Gas Chromatographic Columns," *Microelectromechanical Systems, Journal of,* vol. 16, pp. 853-860, Aug. 2007.
[26] A. Bhushan, D. Yemane, E. B. Overton, J. Goettert, and M. C. Murphy, "Fabrication and Preliminary Results for LiGA Fabricated Nickel Micro Gas Chromatograph Columns," *Journal of Microelectromechanical Systems,* vol. 16, pp. 383-393, April 2007.
[27] A. Bhushan, D. Yemane, D. Trudell, E. Overton, and J. Goettert, "Fabrication of micro-gas chromatograph columns for fast chromatography," *Microsystem Technologies,* vol. 13, pp. 361-368, Feb. 2007.
[28] S. N. Laboratories, "Micro Analytical: Gas - μChemLab," 2008.
[29] J. J. van Deemter, F. J. Zuiderweg, and A. Klinkenberg, "Longitudinal diffusion and resistance to mass transfer as causes of nonideality in chromatography," *Chemical Engineering Science,* vol. 5, pp. 271-289, Sep. 1956.
[30] R. L. Grob and E. F. Barry, "Modern Practice of Gas Chromatography," 4th ed Hoboken: Wiley-Interscience, 2004.
[31] W. L. Jones, "Modifications to the van Deemter Equation for the Height Equivalent to a Theoretical Plate in Gas Chromatography," *Anal. Chem.,* vol. 33, pp. 829-832, June 1961.

[32] G. Gaspar, R. Annino, C. Vidal-Madjar, and G. Guiochon, "Influence of Instrumental Contributions on the Apparent Column Efficiency in High Speed Gas Chromatography," *Anal. Chem.,* vol. 50, pp. 1512-1518, Sep. 1978.
[33] M. J. E. Golay, "The height equivalent to a theoretical plate of retentionless rectangular tubes," *Journal of Chromatography,* vol. 216, pp. 1-8, Oct. 1981.
[34] M. Martin, J.-L. Jurado-Baizaval, and G. Guiochon, "Gas Chromatography in Open Rectangular Channels with Large Aspect Ratios," *Chromatographia,* vol. 16, pp. 98-102, Dec. 1982.
[35] H. D. Papendick and J. Baudisch, "Tapeworm Columns in Gas Chromatography," *Journal of Chromatography,* vol. 122, pp. 443-450, July 1976.
[36] D. Liang, Q. Peng, K. Mitchelson, X. Guan, W. Xing, and J. Cheng, "A Simple and Efficient Approach for Calculating Permeability Coefficients and HETP for Rectangular Columns," *Lab on a Chip,* vol. 7, pp. 1062-1073, Aug. 2007.
[37] J. C. Giddings, "The Role of Lateral Diffusion as a Rate-Controlling Mechanism in Chromatography," *Journal of Chromatography A,* vol. 5, pp. 46-60, 1961.
[38] J. C. Giddings, *Dynamics of Chromatography: Part I. Principles and Theory*. New York: Marcel Dekker, 1965.
[39] J. C. Giddings, "Nonequilibrium Theory of Field-Flow Fractionation," *The Journal of Chemical Physics,* vol. 49, pp. 81-85, July 1968.
[40] J. C. Giddings, J. P. Chang, M. N. Myers, J. M. Davis, and K. D. Caldwell, "Capillary Liquid Chromatography in Field Flow Fractionation-Type Channels," *Journal of Chromatography A,* vol. 255, pp. 359-379, Jan. 1983.
[41] M. L. Hudson, R. Kottenstette, C. M. Matzke, G. C. Frye-Mason, K. A. Schollenberger, D. R. Adkins, and C. C. Wong, "Design, Testing and Simulation of Microscale Gas Chromatography Columns," *Proc. ASME IMECE,* vol. DSC-66, pp. 207-214, 1998.
[42] G. E. Spangler, "Height Equivalent to a Theoretical Plate Theory for Rectangular GC Columns," *Anal. Chem.,* vol. 70, pp. 4805-4816, Nov. 1998.
[43] G. E. Spangler, "Relationships for Modeling the Performance of Rectangular Gas Chromatographic Columns," *Journal of Microcolumn Separations,* vol. 13, pp. 285-292, Nov. 2001.
[44] G. E. Spangler, "Theoretical Approximation for the Linear Flow of Carrier Gas through a Rectangular Gas Chromatogaphic Column," *Analytical Chemistry,* vol. 78, pp. 5205-5207, July 2006.
[45] H. Ahn and S. Brandani, "Analysis of Breakthrough Dynamics in Rectangular Channels of Arbitrary Aspect Ratio," *AIChE Journal,* vol. 51, pp. 1980-1990, July 2005.
[46] J. V. Hinshaw and L. S. Ettre, *Introduction to Open-Tubular Column Gas Chromatography*. Cleveland: Advanstar, 1994.
[47] R. Ghijsen, H. Poppe, J. Kraak, and P. Duysters, "The Mass Loadability of Various Stationary Phases in Gas Chromatography," *Chromatographia,* vol. 27, pp. 60-66, Jan. 1989.
[48] R. Lobinski, V. Sidelnikov, Y. Patrushev, I. Rodriguez, and A. Wasik, "Multicapillary Column Gas Chromatography with Element-Selective Detection," *TrAC Trends in Analytical Chemistry,* vol. 18, pp. 449-460, July 1999.
[49] Rosenkranz, B. Rosenkranz, Bettmer, and J. Bettmer, "Rapid Separation of Elemental Species by Multicapillary GC," *Analytical and Bioanalytical Chemistry,* vol. 373, pp. 461-465, July 2002.

[50] M. v. Lieshout, M. v. Deursen, R. Derks, H.-G. Janssen, and C. Cramers, "A Practical Comparison of Two Recent Strategies for Fast Gas Chromatography: Packed Capillary Columns and Multicapillary Columns," *Journal of Microcolumn Separations,* vol. 11, pp. 155-162, Jan. 1999.
[51] B. He and F. Regnier, "Microfabricated Liquid Chromatography Columns Based on Collocated Monolith Support Structures," *Journal of Pharmaceutical and Biomedical Analysis,* vol. 17, pp. 925-932, Sep. 1998.
[52] B. He, N. Tait, and F. Regnier, "Fabrication of Nanocolumns for Liquid Chromatography," *Analytical Chemistry,* vol. 70, pp. 3790-3797, Sep. 1998.
[53] F. E. Regnier, "Microfabricated Monolith Columns for Liquid Chromatography: Sculpting Supports for Liquid Chromatography," *Journal of High Resolution Chromatography,* vol. 23, pp. 19-26, Jan. 2000.
[54] Y. Saito, K. Jinno, and T. Greibrokk, "Capillary Columns in Liquid Chromatography: Between Conventional Columns and Microchips," *Journal of Separation Science,* vol. 27, pp. 1379-1390, Dec. 2004.
[55] B. E. Slentz, N. A. Penner, E. Lugowska, and F. Regnier, "Nanoliter Capillary Electrochromatography Columns Based on Collocated Monolithic Support Structures Molded in Poly(dimethyl siloxane)," *Electrophoresis,* vol. 22, pp. 3736-3743, Oct. 2001.
[56] B. E. Slentz, N. A. Penner, and F. Regnier, "Geometric Effects of Collocated Monolithic Support Structures on Separation Performance in Microfabricated Systems," *Journal of Separation Science,* vol. 25, pp. 1011-1018, Nov. 2002.
[57] N. Vervoort, J. Billen, P. Gzil, G. V. Baron, and G. Desmet, "Importance and Reduction of the Sidewall-Induced Band-Broadening Effect in Pressure-Driven Microfabricated Columns," *Analytical Chemistry,* vol. 76, pp. 4501-4507, Aug. 2004.
[58] C. T. Culbertson, S. C. Jacobson, and J. M. Ramsey, "Dispersion Sources for Compact Geometries on Microchips," *Analytical Chemistry,* vol. 70, pp. 3781-3789, Sept. 1998.
[59] L.-M. Fu, R.-J. Yang, and G.-B. Lee, "Analysis of Geometry Effects on Band Spreading of Microchip Electrophoresis," *Electrophoresis,* vol. 23, pp. 602-612, Feb. 2002.
[60] S. C. Jacobson, R. Hergenroder, L. B. Koutny, R. J. Warmack, and J. M. Ramsey, "Effects of Injection Schemes and Column Geometry on the Performance of Microchip Electrophoresis Devices," *Analytical Chemistry,* vol. 66, pp. 1107-1113, April 1994.
[61] B. M. Paegel, L. D. Hutt, P. C. Simpson, and R. A. Mathies, "Turn Geometry for Minimizing Band Broadening in Microfabricated Capillary Electrophoresis Channels," *Analytical Chemistry,* vol. 72, pp. 3030-3037, July 2000.
[62] R. Qiao and N. R. Aluru, "Dispersion Control in Nano-Channel Systems by Localized [zeta]-Potential Variations," *Sensors and Actuators A: Physical,* vol. 104, pp. 268-274, May 2003.
[63] S. K. Griffiths and R. H. Nilson, "Low-Dispersion Turns and Junctions for Microchannel Systems," *Analytical Chemistry,* vol. 73, pp. 272-278, Jan. 2001.
[64] A. D. Radadia, R. I. Masel, and M. A. Shannon, "New Column Designs for MicroGC," in *The 14th International Conference on Solid-State Sensors, Actuators and Microsystems*, 2007, pp. 2011-2014.
[65] S. Reidy, D. George, M. Agah, and R. Sacks, "Temperature-Programmed GC Using Silicon Microfabricated Columns with Integrated Heaters and Temperature Sensors," *Analytical Chemistry,* vol. 79, pp. 2911-2917, April 2007.

[66] R. C. Dorf and A. Kusiak, *Handbook of Manufacturing and Automation*. New York: Wiliey, 1994.
[67] P. V. Zant, *Microchip Fabrication: A Practical Guide to Semiconuctor Processing*, 5th ed. New York: McGraw-Hill, 2004.
[68] T. Pandhumsoporn, M. Feldbaum, P. Gadgil, M. Puech, and P. Maquin, "High Etch Rate Anisotropic Deep Silicon Plasma Etching for the Fabrication of Microsensors," in *Micromachining and Microfabrication Pocess Technology II*, Austin, TX, USA, 1996, pp. 94-102.
[69] M. J. Madou, *Fundamentals of Microfabrication: The Science of Miniaturization*, 2nd ed. Boca Raton: CRC Press, 2002.
[70] A. Cozma and B. Puers, "Characterization of the Electrostatic Bonding of Silicon and Pyrex Glass," *Journal of Micromechanics and Microengineering,* vol. 5, pp. 98-102, June 1995.
[71] K. B. Albaugh, P. E. Cade, and D. H. Rasmussen, "Mechanisms of anodic bonding of silicon to pyrex glass," in *IEEE Technical Digest: Solid-State Sensor and Actuator Workshop*, Hilton Head Island, SC, USA, 1988, pp. 109-110.
[72] K. M. Knowles and A. T. J. van Helvoort, "Anodic Bonding," *International Materials Reviews,* vol. 51, pp. 273-311, Oct. 2006.
[73] B. W. Wright, A. Peaden, M. L. Lee, and T. J. Stark, "Free Radical Cross-Linking in The Preparation of Non-Extractable Stationay Phases for Capillary Gas Chromatography," *Journal of Chromatography A,* vol. 248, pp. 17-34, Oct. 1982.
[74] B. E. Richter, J. C. Kuei, N. J. Park, S. J. Crowley, J. S. Bradshaw, and M. L. Lee, "Azo Compounds for Free Radical Crosslinking of Polysiloxane Stationary Phases," *Journal of High Resolution Chromatography,* vol. 6, pp. 371-374, July 1983.
[75] L. Ettre, "Performance of Open Tubular Columns as a Function of Tube Diameter and Liquid Phase Film Thickness," *Chromatographia,* vol. 18, pp. 477-488, Sep. 1984.
[76] S. A. Glantz, *Primer of Biostatistics*, 3rd ed. New York: McGraw Hill, 1992.